

A LABORATORY STUDY TO DEVELOP A PERMEABILITY MODEL FOR
UNCONSOLIDATED GLASS BEAD PACKS BY COMBINING NMR AND SIP
MEASURED PARAMETERS

by

DAVID SAMUEL WALLACE

A Dissertation submitted to the

Graduate School-Newark

Rutgers, The State University of New Jersey

in partial fulfillment of the requirements

for the degree of

Master of Science

Graduate Program in

Environmental Geology

written under the direction of

Dr. Kristina Keating

and approved by

Newark, New Jersey

May, 2015

© 2015

David Samuel Wallace

ALL RIGHTS RESERVED

ABSTRACT OF THE DISSERTATION

A Laboratory Study to Develop a Permeability Model for Unconsolidated Glass Bead

Packs by Combining NMR and SIP Measured Parameters

By DAVID SAMUEL WALLACE

Dissertation Director:

Dr. Kristina Keating

The greatest advantage of geophysical measurements is their ability to quickly, cheaply, and non-invasively provide detailed subsurface information. Therefore, a multitude of research has been conducted to investigate an accurate and robust relationship between geophysical measurements and permeability, a key parameter in any subsurface investigation.

In pursuit of this goal, two methods, Nuclear Magnetic Resonance (NMR) and Spectral Induced Polarization (SIP), have proven to be useful and reliable tools for environmental investigations and permeability estimates. However, as with any geophysical method, NMR and SIP have their weaknesses, namely, the uncertainty associated with indirect measurements of the subsurface. This research explores whether a model that combines NMR and SIP parameters to estimate permeability is more accurate and robust than current models based on NMR and SIP data alone.

In this research, NMR, SIP, and permeability measurements were made on glass bead packs meant to simulate natural unconsolidated aquifer or soil material. The surface roughness and bead size of these beads were altered in order to change the pore scale properties controlling permeability. Bead size appeared to have had a greater influence

than surface roughness on the permeability of the glass bead packs. Measured permeability was compared to a common NMR permeability model and an SIP model designed for unconsolidated material. Both methods performed reasonably well with similar root mean square error (RMSE) and decent correlation with measured permeability. A combined NMR and SIP model was created by utilizing NMR measured peak relaxation time and SIP measured grain size and formation factor, and produced only slightly better estimates of permeability than the single method models.

While a more accurate permeability model could not be formulated for this experiment, combining NMR and SIP data not only produced a comparable permeability model, but also identified the pore scale properties most relevant to the permeability of the glass bead packs.

Acknowledgements

This research was based on work supported by the NSF under Grant No. 1246507. First and foremost, I would like to thank my advisor, Dr. Kristina Keating, who took a novice at geophysics and turned him into a master with her constant wisdom, support, and encouragement. Many thanks to my thesis committee, Dr. Lee Slater, Dr. Andy Binley, and Dr. Dimitris Ntarlagiannis, for their constant support and advice along the way. Special thanks to the other students in the lab, Gordon Osterman, Sam Falzone, Jung Yun, Carl Rosier, and Chi Zhang, I could have not made it through this without their advice, encouragement, and friendship. I would also like to thank all the faculty, staff, and students of the Earth and Environmental Science Department at Rutgers-Newark for their constant advice, support, and friendliness. Last but not least, I thank my wonderful fiancée, Sarah, who has provided me with constant love and encouragement.

Table of Contents

Abstract	ii
Acknowledgements	iv
Table of Contents	v
List of Tables	vi
List of Figures	vii
Introduction	1
Background and Theory	3
Permeability Estimates from Pore Scale Properties	3
Nuclear Magnetic Resonance	5
Spectral Induced Polarization	8
Experimental Procedures	11
Sample Preparation	11
Geophysical Measurements	13
Results	15
Discussion	31
Conclusion	40
References	42
Appendix A	44
Curriculum Vitae	71

List of Tables

Table 1	NMR measured water content results.	16
Table 2	NMR T_2 peak relaxation time results.	17
Table 3	SIP measured formation factor results.	23
Table 4	Mean and standard deviation of 40 frequency sweep phase peak locations.	25

List of Illustrations

Figure 1	Depiction of laboratory NMR principles.	6
Figure 2	Diagram depicting the column used for SIP and NMR measurements.	13
Figure 3	T ₂ relaxation distributions for three replicate samples.	16
Figure 4	Normalized T ₂ relaxation distributions.	18
Figure 5	Conductivity response from example SIP data.	19
Figure 6	Comparison of SIP data from fluid filled and saturated glass bead pack, three week bead leaching test, and linear trends of glass bead leaching over time.	20
Figure 7	Conductivity response from example SIP data after 20 hours.	22
Figure 8	Change in phase peak location over time.	24
Figure 9	First frequency sweep phase peak locations	26
Figure 10	SIP response of <0.05 mm etching cream treated glass beads.	27
Figure 11	SIP response of 0.07-0.11 mm etching cream treated glass beads.	28
Figure 12	SIP response of 0.2-0.3 mm etching cream treated glass beads.	29
Figure 13	Permeability as measured by the laboratory permeameter setup.	30
Figure 14	NMR and SIP parameter relationships with permeability.	34
Figure 15	Comparison of NMR estimated and measured permeability.	36
Figure 16	Comparison of SIP estimated and measured permeability.	37
Figure 17	Comparison of combined method estimated permeability and measured permeability.	39
Figure A-1	SIP response of <0.05 mm etching cream treated glass beads, sample 1	44
Figure A-2	SIP response of <0.05 mm etching cream treated glass beads, sample 2	45

Figure A-3	SIP response of <0.05 mm etching cream treated glass beads, sample 3	46
Figure A-4	SIP response of <0.05 mm 0.1 M HCl treated glass beads, sample 1	47
Figure A-5	SIP response of <0.05 mm 0.1 M HCl treated glass beads, sample 2	48
Figure A-6	SIP response of <0.05 mm 0.1 M HCl treated glass beads, sample 3	49
Figure A-7	SIP response of <0.05 mm 1 M NaOH treated glass beads, sample 1	50
Figure A-8	SIP response of <0.05 mm 1 M NaOH treated glass beads, sample 2	51
Figure A-9	SIP response of <0.05 mm 1 M NaOH treated glass beads, sample 3	52
Figure A-10	SIP response of 0.07-0.11 mm etching cream treated glass beads, sample 1	53
Figure A-11	SIP response of 0.07-0.11 mm etching cream treated glass beads, sample 2	54
Figure A-12	SIP response of 0.07-0.11 mm etching cream treated glass beads, sample 3	55
Figure A-13	SIP response of 0.07-0.11 mm 0.1 M HCl treated glass beads, sample 1	56
Figure A-14	SIP response of 0.07-0.11 mm 0.1 M HCl treated glass beads, sample 2	57
Figure A-15	SIP response of 0.07-0.11mm 0.1 M HCl treated glass beads,	58

	sample 3	
Figure A-16	SIP response of 0.07-0.11 mm 1 M NaOH treated glass beads, sample 1	59
Figure A-17	SIP response of 0.07-0.11 mm 1 M NaOH treated glass beads, sample 2	60
Figure A-18	SIP response of 0.07-0.11 mm 1 M NaOH treated glass beads, sample 3	61
Figure A-19	SIP response of 0.2-0.3 mm etching cream treated glass beads, sample 1	62
Figure A-20	SIP response of 0.2-0.3 mm etching cream treated glass beads, sample 2	63
Figure A-21	SIP response of 0.2-0.3 mm etching cream treated glass beads, sample 3	64
Figure A-22	SIP response of 0.2-0.3 mm 0.1 M HCl treated glass beads, sample 1	65
Figure A-23	SIP response of 0.2-0.3 mm 0.1 M HCl treated glass beads, sample 2	66
Figure A-24	SIP response of 0.2-0.3 mm 0.1 M HCl treated glass beads, sample 3	67
Figure A-25	SIP response of 0.2-0.3 mm 1 M NaOH treated glass beads, sample 1	68
Figure A-26	SIP response of 0.2-0.3 mm 1 M NaOH treated glass beads, sample 2	69
Figure A-27	SIP response of 0.2-0.3 mm 1 M NaOH treated glass beads, sample 3	70

INTRODUCTION

In many environmental investigations or in groundwater and contaminant transport modeling, obtaining a reliable estimate of permeability is crucial for developing an accurate model. Despite their importance, measurements of permeability can be extremely elusive, as the permeability is affected by subsurface heterogeneity and anisotropy. Currently, slug tests or pump tests are industry standards for measuring permeability in near surface investigations. However, these measurements can be costly, time consuming, and may only be representative of a small volume of large environmental sites or aquifers. The field of hydrogeophysics offers an alternative to these more traditional methods by providing relatively quick, non-invasive or minimally invasive, and inexpensive near surface surveys that provide detailed hydrogeological information over large areas. However, while geophysical methods are either non-invasive or minimally invasive, they only provide an indirect measurement, which leads to non-unique results that may not be sensitive to the parameters of interest such as permeability. In fact, geophysical surveys generally need to be coupled with physical sampling to constrain or provide a priori knowledge for geophysical models.

This research focuses on combining two methods, both of which show promise and room for improvement in permeability estimation, to reduce some of the uncertainty associated with the interpretation of single geophysical measurements for permeability estimation: Nuclear magnetic resonance (NMR) and spectral induced polarization (SIP). NMR is a method that uses magnetic fields to align hydrogen protons in water and then measure their relaxation back to their original state. NMR is unique compared to other geophysical methods in that it is directly sensitive to the water content in the subsurface,

and can provide information about porosity. Furthermore, the NMR relaxation time is sensitive to the pore size distribution and has been used for permeability estimation (Weller et al., 2010; Keating, 2014). NMR has also been used for estimating infiltration for groundwater storage recovery (Walsh et al., 2014) and for measuring water content beneath an ice sheet in the cone of an active volcano (Irons et al., 2014).

SIP is an extension of the induced polarization (IP) method. In frequency domain IP measurements, a time varying current applied across a sample and the time varying voltage response is measured and used to determine the complex conductivity. The complex conductivity can be used to estimate the hydraulic properties of that sample, and can provide information on the effective porosity and tortuosity. In SIP measurements, the current is applied at multiple frequencies, which provides additional information about the grain size distribution. With this knowledge, SIP has been studied extensively, for uses ranging from monitoring oil contamination (Cassiani et al., 2009; Schmutz et al., 2010) to estimating the permeability of aquifer material (Slater, 2007; Revil and Florsch, 2010; Weller et al., 2010).

Both NMR and SIP have weaknesses that limit their use. NMR measurements are sensitive to the presence of additional magnetic fields which means that the presence of any paramagnetic mineral interferes with measurements (Keating and Knight, 2007; Keating and Knight, 2010). SIP measurements are sensitive to both changing fluid chemistry and conductive minerals, which make it difficult to interpret SIP results (Lesmes and Frye, 2001).

As these two methods provide similar information about the subsurface, yet have unique sensitivities, there exists the possibility to combine these methods for improved

permeability measurements. **In my research, I tested a permeability model for unconsolidated saturated glass beads with NMR and SIP measured parameters.** *My hypothesis was that a permeability model that combines NMR and SIP parameters is more accurate and robust than current permeability models that use only NMR or SIP parameters alone.*

To test my hypothesis, NMR and SIP measurements were made on saturated glass bead packs. The pore scale properties of the glass beads were altered to influence NMR and SIP measurements and to change permeability. Multiple bead sizes were used to change pore size distribution and the surface area to volume ratio. Surface area treatments were used to increase the surface area to volume ratio without altering the pore size distribution. The results were then used to develop a single robust permeability model for unconsolidated sediments.

Because the physical or chemical properties of the surface are rarely known without invasive or sample consuming experiments, this research aimed to quantify this relationship for future use in fully non-invasive hydrogeophysical surveys.

BACKGROUND AND THEORY

Permeability Estimates from Pore Scale Properties

Most permeability models can trace their roots back to the Kozeny-Carman equation, which relates basic pore scale properties to permeability (Paterson, 1983; Walsh and Brace, 1984).

$$k = \frac{\phi r_h^2}{f\tau} = \frac{\phi}{f\tau S_{por}^2} \quad (1)$$

Here, permeability, k , is related to two variations of the same equation describing the effect of multiple pore properties on the flow of water through a porous system. The

permeability, k , is directly related to both porosity (ϕ), the ratio of void to solid space in a sample, and the pore hydraulic radius, r_h . This hydraulic radius can be related to either the radius of the pore itself or the pore throats, which arguably have a greater influence on permeability. Porosity may also be further defined as mobile and immobile porosity. Some of the pores in a porous system may not be hydraulically connected to the rest of the pore space, meaning that they will not contribute to the flow or permeability of a system. These pores would be described as part of the immobile porosity, whereas the pores contributing to flow and permeability would be described as the mobile porosity. These are distinctions to keep in mind when determining how geophysical methods determine porosity. For example, electrical methods such as SIP depend on the propagation of current through a pore system, and therefore would be sensitive to only the connected mobile porosity. However, NMR's direct sensitivity to the total water content in a sample means that it cannot distinguish between mobile and immobile porosity.

The remaining terms share an inverse relationship with k , meaning that their increase will lead to a decrease in k . Tortuosity, τ , is a measure of the increased travel distance water must flow through a long, tortuous path winding through the saturated voids of a porous system. The more tortuous the path, the greater the influence friction may have on water in the system, causing a decrease in permeability. The shape factor, f , is simply a factor to take into account the effect of the shape of soil or mineral particles on the pore geometry and flow of a porous system. Spherical particles might pack more regularly and provide greater pore space than plate shaped clays that may increase the tortuosity and decrease the permeability of a porous system. Finally, S_{por} , or the surface

area to volume ratio, will have a strong influence on permeability as well. Increasing the surface area, or surface roughness, of a porous system, without changing its volume will increase the influence of friction upon water flow through the pore system, thereby decreasing the permeability of the system.

By altering the physical properties of glass bead packs, we can alter some of these pore scale properties and observe their influence on not only permeability, but NMR and SIP measurements as well. Changing the bead sizes used in the experiment changes S_{por} by changing the pore volume and r_h of the pore system. Altering the surface roughness of the glass beads through etching treatments increases S_{por} without changing r_h or ϕ .

Nuclear Magnetic Resonance

In laboratory NMR, a sample is placed inside a static magnetic field and the spin magnetic moment of the protons, or hydrogen atoms in water, align with the static magnetic field. A secondary magnetic field oscillating at the Larmor frequency is then applied. The Larmor frequency is tuned specifically to detect the spin magnetic moment of hydrogen protons. When the secondary field is removed, the protons return, or relax, back to alignment with the static magnetic field (Figure 1).

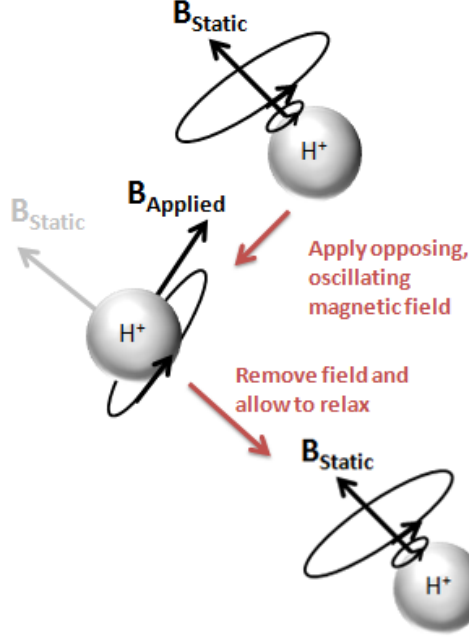


Figure 1: The principles of laboratory NMR.

The signal measured in a material with a range of pore sizes is a time dependent, nuclear magnetization $M(t)$, which is described as a multiexponential decay:

$$M(t) = \sum_i m_i e^{-t/T_{2i}} \quad (2)$$

where m_i is proportional to the number of protons relaxing at time T_{2i} ; m_i is typically plotted versus T_{2i} to give the relaxation time distribution. The initial amplitude, $M(0)$, is proportional to the total number of protons relaxing, which is related to the total water content of the sample. If the volume of the sample is known and the sample is fully saturated, the porosity can be calculated using this relationship.

For simplicity, the relaxation time distribution is often represented by a single relaxation time. This can be the mean log of the relaxation time distribution, T_{2ml} , the median of the relaxation time distribution, T_{2md} , or the peak of the relaxation time distribution, T_{2pk} . The inverse of this representative relaxation time is the relaxation rate, T_2^{-1} . The relaxation rate is described as:

$$T_2^{-1} = T_{2B}^{-1} + T_{2S}^{-1} + T_{2D}^{-1} \quad (3)$$

where T_{2B}^{-1} , is the fluid relaxation rate and depends on dipole-dipole molecular interactions, T_{2S}^{-1} is the surface relaxation rate and corresponds to water relaxing in response to contact with the pore surfaces, and T_{2D}^{-1} is the diffusion relaxation rate caused by magnetic field inhomogeneities present in the sample (Keating and Knight, 2007). By measuring at different echo times, we can account for T_{2D}^{-1} . The echo time is the amount of time between the magnetization pulses that refocus the spin magnetic moment of protons. If magnetic field inhomogeneities exist in the sample, then the spin of some protons will decay to various degrees in this time. In this case, our signal would vary with echo time, and we must account for T_{2D}^{-1} . If no difference exists between the different echo time measurements, T_{2D}^{-1} can be ignored. The surface relaxation rate is especially important because it is related to the surface area to volume ratio:

$$T_{2S}^{-1} = \rho_2 * S_{por} \quad (4)$$

where S_{por} is the surface area to volume ratio of the porous media and ρ_2 is the surface relaxivity, related to the amount of paramagnetic species with unpaired electron spins accessible by hydrogen protons in porous media. ρ_2 values are influenced by the concentration of paramagnetic species on the surface of the mineral grain (Keating and Knight, 2007). This complicates NMR measurements because unless the surface relaxivity is known, physical samples must be taken to determine ρ_2 as the NMR response will change with differences in lithology.

With information such as porosity and S_{por} , a permeability method can be estimated with NMR data. The Schlumberger-Doll-Research (SDR) model is a common formula for NMR that uses two parameters taken directly from NMR data, T_{2pk} and porosity, ϕ (Coates et al., 1999).

$$k = a_2 T_{2pk}^2 \phi^4 \quad (5)$$

Here T_{2pk} is chosen in place of T_{2ml} , the value commonly used for this equation, because it is not influenced by signal from bulk water, which is only an indication of imperfect packing at the top of the columns and has no relation to the pore structure of the packed column. Altering the properties of glass bead packs should influence this equation in two ways. First, including multiple bead size ranges in the experiment changes S_{por} in each of the samples, altering the peak relaxation time (equation 5). Second, the etching treatments increase the surface area of the grains, increasing S_{por} without changing the volume of the samples. Equation 5 was designed specifically for consolidated sediments whose signals are dominated by T_{2s}^{-1} (i.e., $T_{2s}^{-1} \gg T_{2B}^{-1}$); in unconsolidated sediments, where T_{2B}^{-1} can be on the same order of magnitude as T_{2s}^{-1} , the equation must be modified to account for T_{2B}^{-1} (Dlubac et al., 2013):

$$k = a_2 \left(\frac{1}{T_{2pk}} - \frac{1}{T_{2B}} \right)^{-2} \phi^4 \quad (6)$$

While the advantage of this model is that NMR is very sensitive to changes in S_{por} , this also means that the model will vary for changes in ρ_2 , or paramagnetic species in the mineral grain, which may or may not actually change permeability. Additionally, while changes in surface area might not affect permeability significantly, they could alter T_2 signals to the extent that an accurate permeability estimate cannot be made.

Spectral Induced Polarization

Induced polarization (IP) works on the principles of electromigration and polarization. When a current is applied to a sample, ions in solution electromigrate along the direction of the current through the fluid. When the current reaches a mineral grain,

ions in the electrical double layer (EDL) electromigrate through the EDL to the other side of the mineral grain thereby polarizing the grain. Once the current is removed, the ions begin to relax back to their original distribution. Because the relaxation of ions is not instantaneous, we can measure the phase lag between the voltage drop from the end of the applied current and the relaxation of ions in solution. Spectral IP (SIP) measurements are made by applying a sinusoidal, alternating current to a sample through a spectrum of frequencies. These different frequencies will polarize different sized particles, creating a relationship between the SIP response and the grain size.

In SIP measurements, the magnitude of the complex conductivity and the phase lag of the sample are measured. The phase lag is the difference between the measured voltage and the applied sinusoidal due to the relaxation of the ions. The phase lag, φ , and the magnitude, $|\sigma|$, can be used to calculate the real and imaginary components of the complex conductivity (σ' and σ'' respectively):

$$|\sigma| = \sqrt{(\sigma')^2 + (\sigma'')^2} \quad (7)$$

$$\varphi = \tan^{-1}\left(\frac{\sigma''}{\sigma'}\right) \approx \frac{\sigma''}{\sigma'} \quad (8)$$

Waxman and Smits (1968) describe the real part of the conductivity with:

$$\sigma' = \sigma_{el} + \sigma'_{surf} = \frac{1}{F}\sigma_w + \sigma'_{surf} \quad (9)$$

where σ_{el} is the electromigration, or bulk fluid conductivity, σ'_{surf} is the surface conductivity, F is the electrical formation factor, and σ_w is the pore fluid conductivity.

The formation factor is a measure of the ratio of the conductivity of the formation to the conductivity of the saturating fluid. Therefore, we are able to measure F by calculating the slope of a line generated by plotting the fluid conductivity versus the conductivity of the system as measured by SIP. For a simple system such as unconsolidated glass bead

packs, the relationship between fluid and bulk conductivity is assumed to be linear above low fluid conductivities (Archie, 1942). The formation factor is related to both the tortuosity of a system and the porosity:

$$F = \phi^{-m} \quad (10)$$

where m is the cementation exponent of the rock or soil, which describes the influence of porosity on the conductivity (Archie, 1942).

Fundamentally, permeability can be related to electrical parameters through a length scale L , Archie's formation factor F (1942) related to the tortuosity of the system, and an empirical constant c (Katz and Thompson, 1986):

$$k = c \frac{L^2}{F} \quad (11)$$

Revil and Florsch (2010) defined a variation on this model specifically for unconsolidated sediments or glass bead packs:

$$k = \frac{D_i \tau}{9F^3} \quad (12)$$

where D_i is the diffusion coefficient of the water and τ is defined as the SIP relaxation time (inverse of frequency), which is related to the grain size of the system.

The diffusion coefficient of water in a normal room temperature laboratory (25°C) is $2.13 \times 10^{-5} \text{ cm}^2 \text{ s}^{-1}$ (Simpson and Carr, 1958). The SIP relaxation time is related to grain size, d , through equation 13:

$$\tau = \frac{d^2}{8D_i} \quad (13)$$

Porosities and cementation factors should not vary significantly within unconsolidated glass bead packs, which means that F should not play a strong role in permeability estimation.

Revil and Florsch's (2010) permeability method based on electrical parameters performs well in situations where conditions favor their use. However, electrical methods break down when measurements of F are not available or unreliable and where fluid conductivity is too variable or unknown (Lesmes and Frye, 2001).

EXPERIMENTAL PROCEDURES

Sample Preparation

Soda lime glass beads (Jencons) of known particle sizes took the place of sand or aquifer material to simulate unconsolidated aquifer material with measurement repeatability and standardization in the laboratory. Three glass bead samples, ranging in size from fine silt to medium sand were chosen: <0.05 mm, 0.07-0.11 mm, and 0.2-0.3 mm. Previous research has shown that etching the surfaces of these glass beads alters S_{por} , which in turn perturbs the NMR and possibly the SIP signals (Leroy et al., 2008; Keating, 2014).

These three bead sizes were treated with three surface area treatments shown to alter surface roughness: 0.1 M hydrochloric acid bath (AW), 1 M sodium hydroxide bath (BE), and treatment with a common, commercially available glass etching cream (EC) (Armor Etch, active ingredient hydrofluoric acid) (Keating, 2014). The HCl treatment was intended to remove any paramagnetic impurities from the glass beads that might affect NMR measurements, resulting in a smooth bead (Bryar and Knight, 2003). The NaOH treatment was expected to etch the beads to increase the surface area without decreasing the diameter or shape of the glass bead (Zengin et al., 2006). The

commercially available etching cream provided a third method also shown to effectively alter the surface area of glass beads (Keating, 2014).

Beads treated with the 1 M NaOH and 0.1 M HCl solutions were treated by placing them in the solution on a shaker set to 350 rpm for 1 hour. EC treated beads were mixed manually with the etching cream for one minute, rinsed with DI water until the decanted solution was visually clear, then repeatedly rinsed with acetone to remove any remaining cream. The beads were then air dried, rinsed again with DI water, and oven dried at 80°C overnight. Then, all of the soda lime beads were set in DI water for five weeks in an attempt to leach out any alkali ions that might affect the SIP signal response.

Beads were packed inside a clear cast acrylic cylinder with an inner volume of approximately 190 cm³ (Figure 2). To prevent any air from being trapped in the sample, beads were packed and saturated simultaneously by pouring a small layer of beads (approx. ½ cm) into the bottom of the cylinder and then saturated from below. This procedure was repeated until the entire cylinder was packed and saturated without any air bubbles. Columns were saturated by attaching the bottom of the column to a fluid reservoir via 1/16" inner diameter clear Tygon PVC tubing and ferrule connected to the bottom cap of the column (Figure 2). An 11 µm filter paper was attached to the ferrules connecting to both the top and bottom caps to allow the columns to be filled entirely with the glass beads without the beads spilling into the connecting tubes. Porous wooden plugs separated the interior of the column from the electrode ports to prevent movement of glass beads but allowed fluid to flow to the potential electrodes in an SIP setup. When capping the sample tube, hydraulic head was applied to the bottom of the sample, and an open cap was placed on so that air might escape the sample tube upon capping. There

must be no air bubbles present in the top or bottom of the caps as they would interfere with the electrical connection between the electrodes in the caps and the column's saturating fluid.

After the NMR and laboratory permeability measurements were made, all samples were saturated with a single salt solution (NaCl) with a fluid conductivity of 0.1 mS/cm. Glass bead dissolution, described later, negated the use of additional conductivity solutions. Sodium chloride (NaCl) solutions were prepared by first boiling deionized water to degas the solution. Then, NaCl was added and conductivity was measured simultaneously until the desired conductivity solution was reached. A peristaltic pump was used to flow water through the columns until the outflow conductivity reached equilibrium ($\pm 1\%$ of previous measurement).

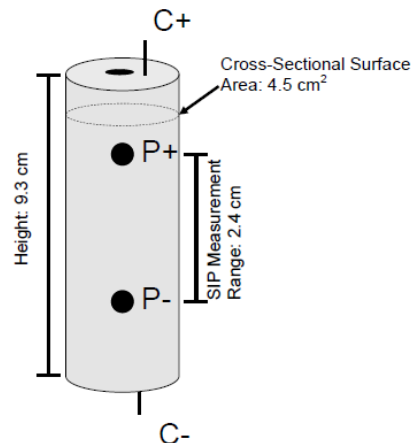


Figure 2: Simplified diagram depicting the column used for both SIP and NMR measurements. Silver-silver chloride electrodes that minimize electromagnetic coupling are present as coils in both the top and bottom caps. Potential electrodes are placed in removable plugs that provide contact during SIP measurements, but can be removed for placement inside the NMR instrument.

Geophysical Measurements

After packing and saturation, the columns were capped and prepped for NMR measurements. This preparation included plugging the top and bottom column caps and

leaving the side ports open to fit into the instrument, a Magritek 2 MHz Rock Core Analyzer. Fluid and beads were kept in place by porous wooden plugs placed inside the side ports. NMR measurements were made at four echo times (200, 400, 800, and 1600 μs) to test that the diffusion relaxation time was negligible and were repeated three times to ensure accuracy. Raw data was inverted to determine the relaxation time distributions using a non-negative least squares (NNLS) algorithm. NNLS was chosen because it involves a least squares inversion with the constraint that a lower bound for model parameters is set to zero, as we realistically cannot have negative NMR signals (Aster et al., 2013). NMR estimated water content, θ_w , was calculated through the direct measurement of water content in the columns. A calibration curve was created by plotting NMR initial signal amplitude versus samples with known water contents. The slope of this curve was then used to relate the initial signal amplitude of any sample to its water content.

After NMR measurements were made, the column was attached to a laboratory permeameter setup to measure permeability. A constant head permeability setup was created by elevating a reservoir of water above the sample, allowing water to flow from the reservoir down through the top of the column. Outflow was measured through the bottom, and hydraulic head was measured using two manometers attached to the two SIP measurement ports on the side of the column.

Upon completion of the permeability measurements, the columns were flushed with the salt solution as described above and prepared for SIP measurements. Measurements were made immediately after saturation with the last conductivity measurement taken to be the fluid conductivity. Silver-silver chloride electrodes were

attached to the side ports of the sample columns in such a way that they just touch the porous wooden plugs separating the inside and outside of the column. The column was then placed upright on a stand, current and potential electrodes attached as shown in Figure 2, and current injected at frequencies ranging from 0.01 to 1000 Hz in 26 log-spaced steps such that there were 5 measurements per decade. Measurements were made using a portable SIP field/lab unit (Ontash & Ermac) with a phase accuracy of less than 1 mRad and a 1 mHz to 20 kHz measurement range capability. In order to capture any changes in SIP response over time due to bead dissolution, measurements were repeated 40 consecutive times, spanning a range of 20 hours. Immediately after SIP measurements concluded, the columns were weighed to both ensure no appreciable loss of water and to allow for a calculation of gravimetric water content. Then, the fluid inside the column was flushed to determine the final fluid conductivity inside the column after 20 hours of SIP measurements. The volumetric water content was calculated from:

$$\theta_w = \frac{V_w}{\pi r^2 H} \quad (14)$$

where V_w is the volume of water in the sample, r is the radius of the column (1.176 cm), and H is the height of the column (9.271 cm).

RESULTS

The volumetric water content measurements determined from the NMR data indicate the columns were packed consistently. Across all samples, NMR measured θ_w ranged from 0.273 to 0.334 with a mean of 0.306 and standard deviation of 0.017. Table 1 shows the range of θ_w for the columns.

Table 1: Volumetric water content (θ_w) as measured by NMR for each glass bead sample, average θ_w , and standard deviation the three replicate samples.

	Volumetric Water Content ($\text{cm}^3 \text{cm}^{-3}$)								
	<u>$\leq 0.05 \text{ mm}$</u>			<u>$0.07\text{-}0.11 \text{ mm}$</u>			<u>$0.2\text{-}0.3 \text{ mm}$</u>		
	AW	BE	EC	AW	BE	EC	AW	BE	EC
Sample 1	0.273	0.306	0.329	0.318	0.298	0.285	0.314	0.314	0.296
Sample 2	0.291	0.284	0.329	0.310	0.316	0.289	0.312	0.320	0.301
Sample 3	0.298	0.279	0.334	0.320	0.318	0.283	0.317	0.296	0.323
Average	0.288	0.290	0.331	0.316	0.310	0.286	0.314	0.310	0.306
Std. Dev	0.013	0.015	0.003	0.005	0.011	0.003	0.002	0.012	0.014

Additionally, because water content can be directly determined from NMR measurements, the T_2 distributions from the three replicate samples were used to assess the consistency of the packing. Figure 3 shows an example of the typical variation between columns packed with 0.07 to 0.11 mm EC treated beads. This variation was found to be representative of all bead sizes and treatments, indicating that packing was consistent.

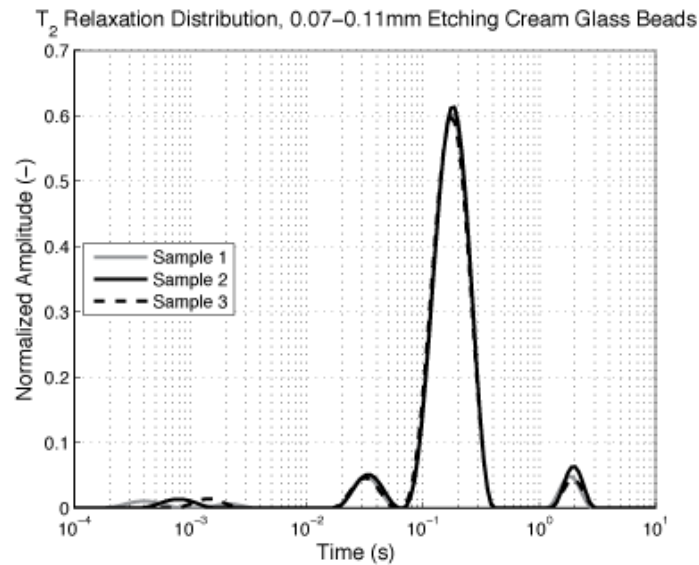


Figure 3: T_2 relaxation distribution for three replicate 0.07-0.11 mm etching cream treated glass bead packs. The amplitude normalized by the initial signal magnitude.

NMR results also suggest that the surface area treatments measurably increased the surface area of all glass bead sizes. Table 2 shows the NMR T_{2pk} relaxation time, an indirect indicator of surface area to volume ratio (equation 4).

Table 2: NMR T_2 peak relaxation time for each glass bead sample and the average and standard deviation for the three replicate samples.

	T_{2pk} (s)								
	<u>< 0.05 mm</u>			<u>0.07-0.11 mm</u>			<u>0.2-0.3 mm</u>		
	AW	BE	EC	AW	BE	EC	AW	BE	EC
Sample 1	0.096	0.058	0.166	0.316	0.138	0.174	0.631	0.398	0.832
Sample 2	0.100	0.058	0.120	0.302	0.138	0.182	0.661	0.398	0.794
Sample 3	0.120	0.076	0.126	0.316	0.145	0.174	0.661	0.380	0.832
Average	0.105	0.064	0.137	0.311	0.140	0.177	0.651	0.392	0.819
Std. Dev	0.013	0.011	0.025	0.008	0.004	0.005	0.017	0.010	0.022

As expected, the acid washed treatment (AW) had higher T_{2pk} relaxation times than the base treatment (BE), which coincides with the thought that the AW treatment did not etch the surface of the beads, only removed any remaining paramagnetics. However, etching cream treated beads (EC) had greater relaxation times than the acid washed, perhaps because the acetone rinse didn't fully remove the etching cream. Remaining cream might cover any surface roughness of the bead, resulting in a smoother bead than expected. The acetone wash was expected to dissolve any residual etching cream so it could be washed away more easily, but it appears as if the treatment was not as effective as anticipated.

Figure 4 shows the T_2 relaxation distributions for each bead size and each treatment averaged across the three replicate samples. This provides the single NMR distributions for each sample shown in Figure 4. This graph can be compared to Keating (2014), showing that this research produced comparable changes in surface roughness for bead sizes and treatments. The only differences to note are with the etching cream

treated samples. This research added an additional step involving acetone washing in an attempt to remove more residual etching cream.

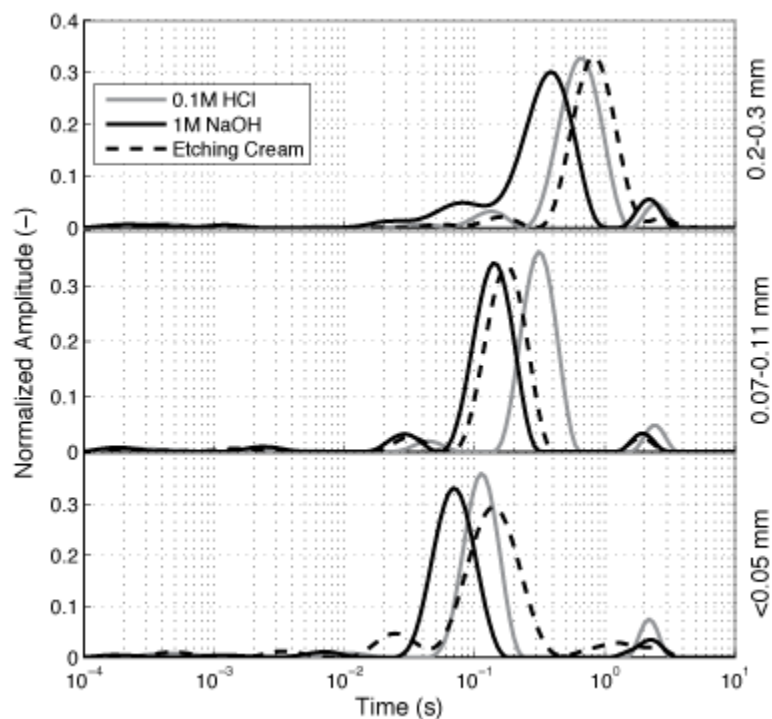


Figure 4: The NMR T_2 distributions normalized by the initial signal magnitude. Each distribution is the average value of the three replicate samples.

The SIP results proved more complicated than the NMR results. At first glance, we observe an unrealistic increase in conductivity with decreasing frequency. Figure 5 is an example of a typical frequency sweep for a saturated glass bead pack used in this experiment.

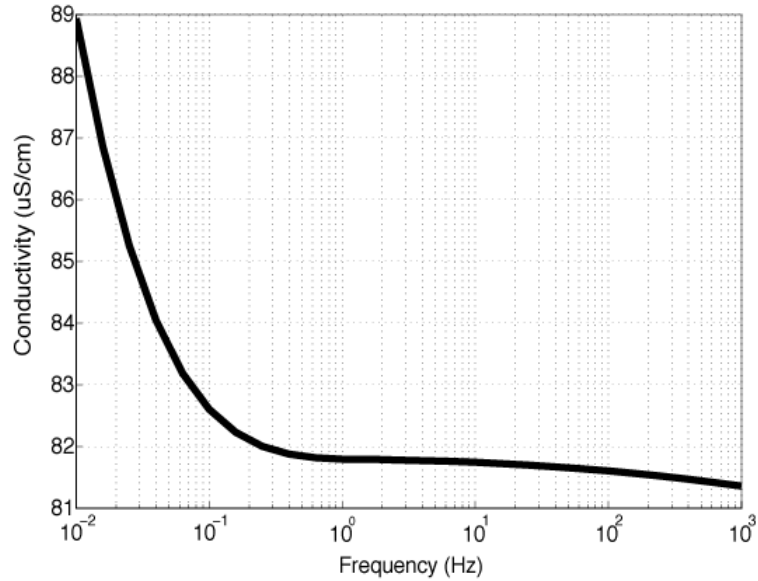


Figure 5: An example conductivity response. The data shown was collected on the etching cream treated glass beads using frequencies ranging from 0.01 to 1000 Hz.

When the SIP measurement is repeated over the course of 20 hours, the conductivity of the glass bead columns continually increased as a function of time in contrast to a sample with only an electrolyte solution (Figure 6a). This indicates that some process occurred within the columns that increased their conductivity over time. To test any influence of glass beads on fluid conductivity apart from SIP, a small sample of glass beads (approximately 20 g) was soaked in a 0.1 mS/cm NaCl solution (approximately 40 mL), and conductivity measurements of the saturating fluid were taken over a period of three weeks. Surprisingly, it was found that the conductivity of the solution steadily increased over time after a sharp increase in the first 24 hours of sampling (Figure 6b).

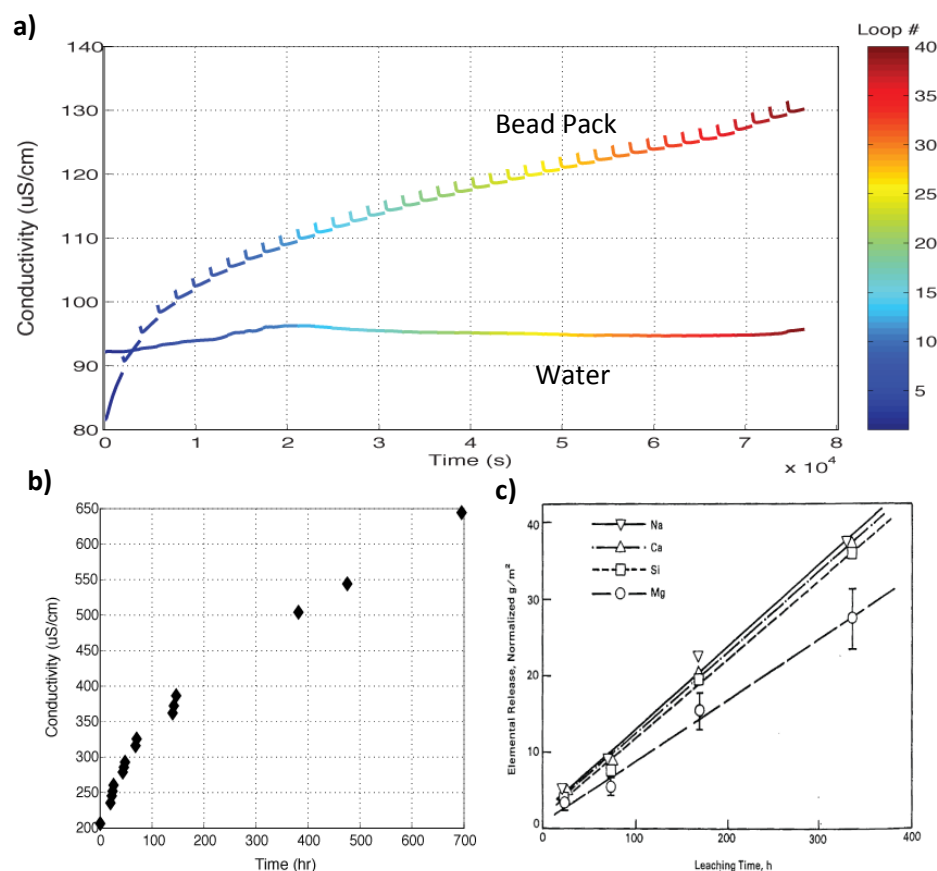


Figure 6: a) SIP measured sample conductivity of a column filled with only 100 $\mu\text{S/cm}$ NaCl and a saturated column packed with <0.05 mm etching cream treated glass beads b) Conductivity measurements over time of 20 g of glass beads sitting in 40 mL of 100 $\mu\text{S/cm}$ NaCl solution c) Linear trends of glass bead leaching over time for four components of soda lime glass (Pederson, 1986)

Previous studies have shown that glass is not as stable a material as commonly thought, especially when it is submerged in water and its surface area is increased significantly (Figure 6c) (Doremus, 1975; Lanford et al., 1979; Pederson et al., 1986). The reason why glass is not as inherently stable as we might expect is due to its chemical composition. Common glass, as used in this experiment, is referred to as “soda lime” glass, which contains only approximately 75% silicon dioxide, with the rest being highly soluble oxides such as sodium oxide and calcium oxide. Other higher silica content glasses exist, such as borosilicate glass, but are not readily available in the quantity and

grain size needed for this study. When in contact with water, the sodium and other highly soluble cations in the soda lime glass dissolve into solution in an attempt to reach equilibrium with the saturating solution. These cations are replaced with hydronium molecules from the water, which in turn reduce the pH of the saturating solution. Because of the high solubility of sodium and other cations in the glass, equilibrium was never truly reached in the saturated glass bead columns saturated at lower, more natural conditions, so these measurements were in a constant state of flux. Despite this substitution, we should also expect glass beads to have similar electrical double layers (EDL) as sand grains. The substitution occurring in the glass should not change the charge as it does with isomorphic substitution in clays, which lead to higher charge densities and greater cation exchange capacities. This leads to a weaker, but still measureable SIP signal response similar to that seen in sands. Despite these issues, glass beads served well as a testable proxy for unconsolidated aquifer material with known grain sizes and whose properties may be altered using proven methods.

To solve the issue of glass bead dissolution interfering with SIP signals, all samples were run on the SIP instrument for 20 hours, or 40 frequency sweeps from 1000 to 0.01 Hz with 26 logarithmically spaced steps. The first sweep contains valuable information about phase peak location and relaxation times but has poor conductivity data due to bead dissolution (Figure 5). However, after 20 hours the phase peak has dropped due to increased conductivity, but due to the conductivity stabilization seen in Figure 6a, the conductivity data of the last sweep contains more realistic data (Figure 7). We still observe some increase in conductivity at lower frequencies due to the length, but this response is minimal relative to the rest of the data.

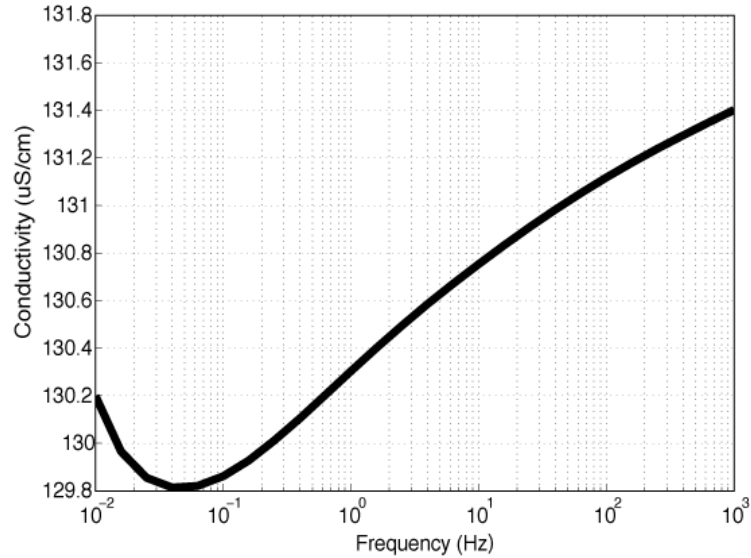


Figure 7: An example of conductivity response. The data was the 40th frequency sweep collected on the <0.05 mm etching cream treated glass beads for frequencies ranging from 0.01 to 1000 Hz.

Despite these issues, we can actually use this bead dissolution to our advantage by using the increased sample and fluid conductivity over time as a high conductivity sample. Assuming that bead dissolution simply increases the pore fluid conductivity and does not etch the glass beads in any way, we can calculate formation factor with our low fluid and sample conductivities at the beginning of SIP testing, and the high fluid and sample conductivities at the end of SIP testing. By dividing the change in fluid conductivity by the change in sample conductivity and assuming a linear relationship, we determine Archie's (1942) formation factor. Table 3 lists the formation factor values determined using this process for all samples.

Table 3: Formation factor estimates for each glass bead sample as well as the average and standard deviation from the three replicate samples.

	Formation Factor (-)								
	<u>< 0.05 mm</u>			<u>0.07-0.11 mm</u>			<u>0.2-0.3 mm</u>		
	AW	BE	EC	AW	BE	EC	AW	BE	EC
Sample 1	6.21	5.16	7.87	5.15	4.27	4.50	4.34	5.54	6.31
Sample 2	5.37	4.73	4.94	5.24	4.54	4.96	4.49	5.44	4.59
Sample 3	5.92	5.66	5.84	4.49	4.37	5.28	4.53	4.00	4.15
Average	5.83	5.18	6.22	4.96	4.39	4.91	4.45	4.99	5.02
Std. Dev	0.43	0.47	1.50	0.41	0.14	0.39	0.10	0.86	1.14

While this method of estimating formation factor might work in theory, there are several issues worth mentioning that affect the data. First, the conductivity change of the sample and pore fluid are relatively small, and only represent a limited range of conductivity we may see in a sample. Second, formation factor should not vary much in unconsolidated sediments as they have higher porosities and therefore have a smaller influence from the formation than consolidated material. Despite the questionability of the formation factor results, the values are within the range specified by the SIP model. Revil and Florsch (2010) found a cementation factor of 1.3 to 1.5 for their unconsolidated sediments, and using the porosity range found in Table 1 we can estimate the ranges of what formation factor should be using equation 10. With this relationship, formation factors for the glass bead samples should range from 4.2 to 7.0, and in fact we do observe a similar range of values for the formation factor measured in this experiment (Table 3). However, as comparable as the formation factor estimates may be, they are still within a small range and may have a significant amount of uncertainty associated with them.

Additionally, as different frequencies polarize different sized particles, the peak relaxation time can be related to the particle size in a given sample. A phase peak at lower frequencies would indicate larger grain sizes, and likewise, a phase peak at higher

frequencies would indicate smaller grain sizes. While the conductivity change over the 20 hour sampling period may diminish phase peak magnitude, there appears to be little to no influence on phase peak location. Figure 8 shows the change in phase peak over time of a representative sample, and Table 4 shows the mean phase peak location over 40 frequency sweeps and the associated standard deviation. Comparing the phase peak location in Figure 8 to the conductivity change of the sample in Figure 6, we observe a slight increase in the phase peak location, but we do not observe a systematic, continual increase associated with the conductivity change in the sample.

The phase peak from the first frequency sweep will be utilized for analysis as it has been shown that phase peak shows no significant changes. Additionally, we observe some increased noise during 20 hours of data collection, and we lose some of the distinctness of the phase peak as magnitude decreases over time with increasing conductivity, so choosing the mean peak location across 40 frequency sweeps may lead to some loss in accuracy.

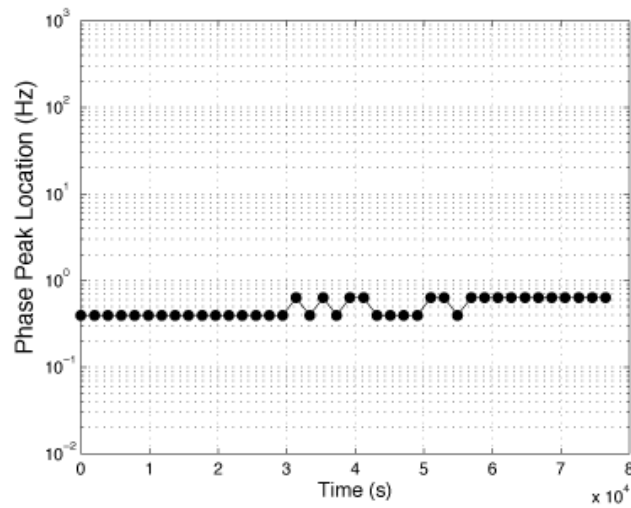


Figure 8: Phase peak location in Hz vs. frequency sweep time for the 40 frequency sweeps.

Table 4: Mean and standard deviation of phase peak locations in Hz for each glass bead sample over the 40 frequency sweeps.

	Phase Peak Change (Hz)								
	< 0.05 mm			0.07-0.11 mm			0.2-0.3 mm		
	AW	BE	EC	AW	BE	EC	AW	BE	EC
Sample 1	3.34 ±	2.36 ±	0.40 ±	1.01 ±	0.70 ±	0.47 ±	0.09 ±	0.75 ±	0.14 ±
	0.88	0.81	0	0.47	0.15	0.11	0.03	0.41	0.04
Sample 2	4.69 ±	2.48 ±	0.50 ±	1.77 ±	0.99 ±	0.54 ±	0.08 ±	0.11 ±	0.10 ±
	1.86	0.76	0.12	0.57	0.06	0.12	0.04	0.03	0.03
Sample 3	4.46 ±	2.95 ±	0.63 ±	1.79 ±	2.71 ±	0.55 ±	0.08 ±	0.29 ±	0.22 ±
	1.33	0.68	0	0.62	2.50	0.14	0.02	0.25	0.16

With the average phase peak shown in Figure 9, we see a relationship between bead size and phase peak despite the effects of bead dissolution. Peak locations were calculated using a model fit to the first frequency sweep of data. The peak phase value in the 0.05 to 10 Hz range was located and then a curve was fit to the three points on either side of the peak value. Then, the peak location of this modeled curve was chosen so that I was not limited to the five sample points per decade for my phase peak location, which allowed for a more accurate estimation of phase peak. Phase values in the 0.01 to 0.05 and 10 to 1000 Hz range were discounted as they generally contained noise from the polarization of the electrodes. However, I continued to sample in this range so I could observe trends in the data and determine the peak location manually if noise was too great for the curve fitting method.

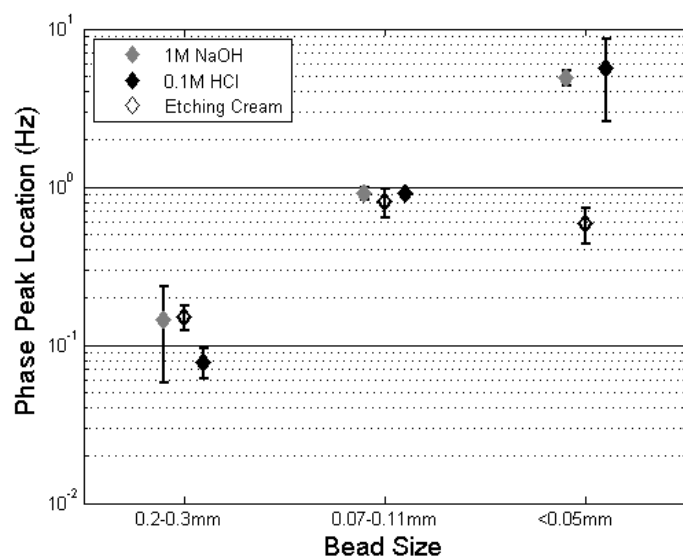


Figure 9: Average and standard deviation of the first frequency sweep phase peak location for each bead size and treatment.

Graphically representing the SIP results proves more difficult than the NMR results. Because there are 40 frequency sweeps (collected from 1000 to 0.01 Hz) for three replicate columns of three different bead treatments and three different bead sizes, only representative spectra will be presented here. The complete SIP datasets can be found in Appendix A. Figures 10 through 12 show the change in phase, sample conductivity, real conductivity, and imaginary conductivity over 40 sequential 1000 to 0.01 Hz frequency sweeps for etching cream treated beads of three different sizes.

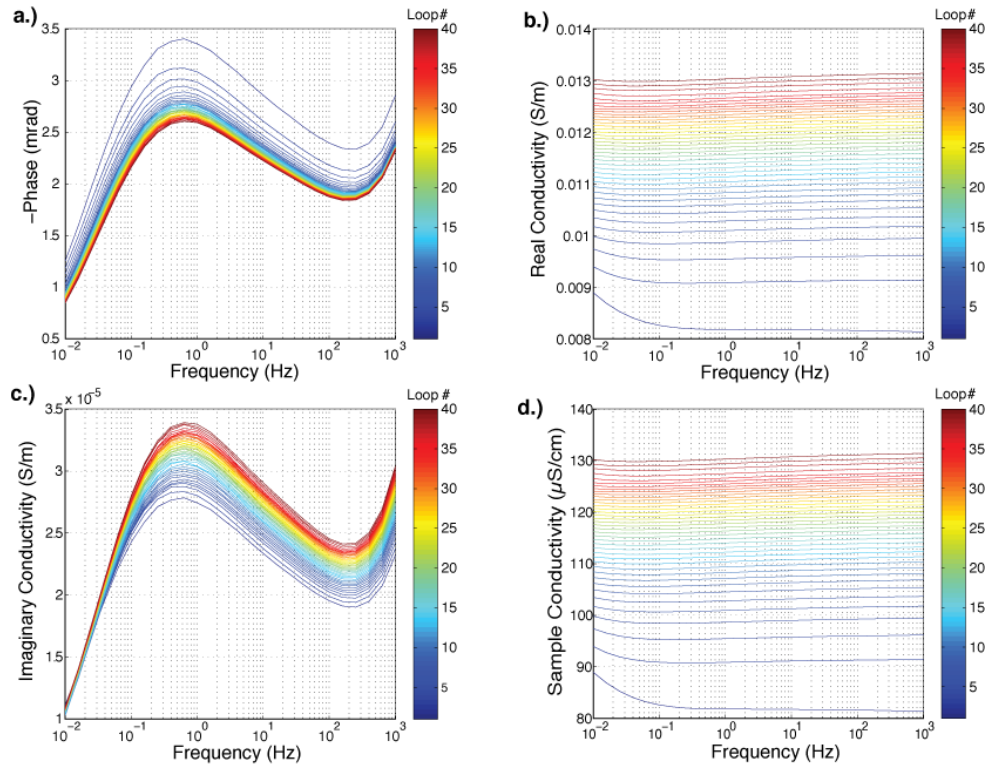


Figure 10: SIP response of <0.05 mm etching cream treated glass beads over 40 frequency sweeps from 1000 to 0.01 Hz with 26 log-spaced steps. a) phase in negative milliradians b) real component of the complex conductivity in S/m c) imaginary component of the complex conductivity in S/m and d) sample conductivity in $\mu\text{S/cm}$.

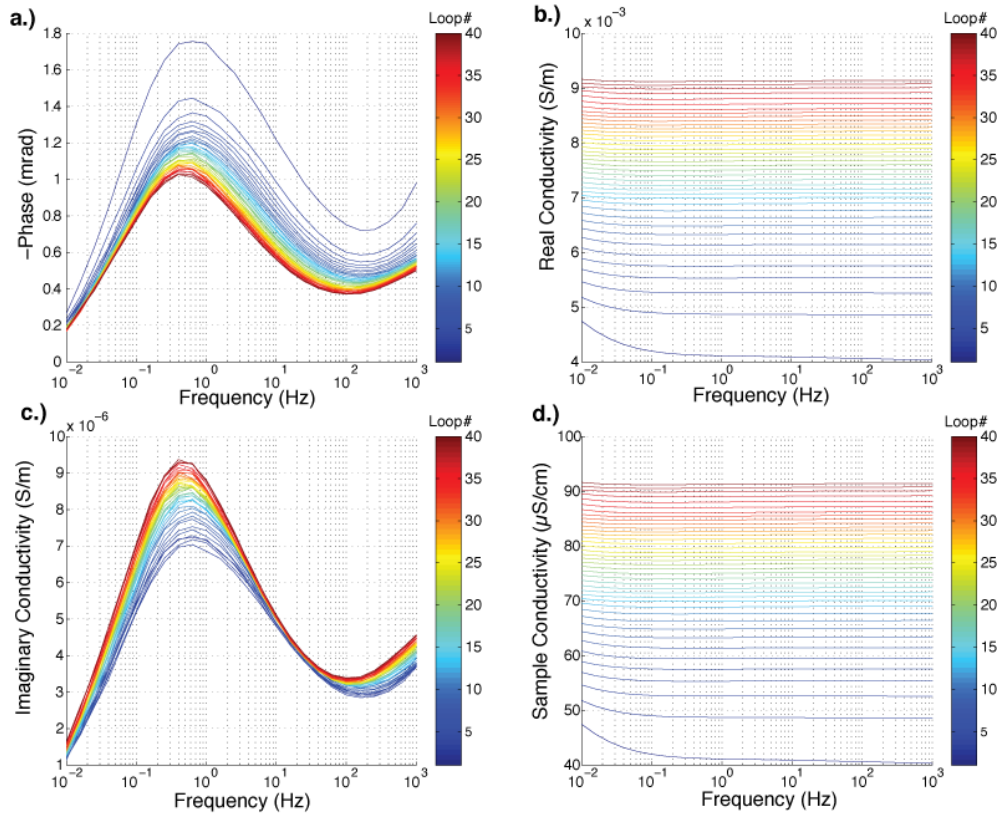


Figure 11: SIP response of 0.07-0.11 mm etching cream treated glass beads over 40 frequency sweeps from 1000 to 0.01 Hz with 26 log-spaced steps. a) phase in negative milliradians b) real component of the complex conductivity in S/m c) imaginary component of the complex conductivity in S/m and d) sample conductivity in μ S/cm.

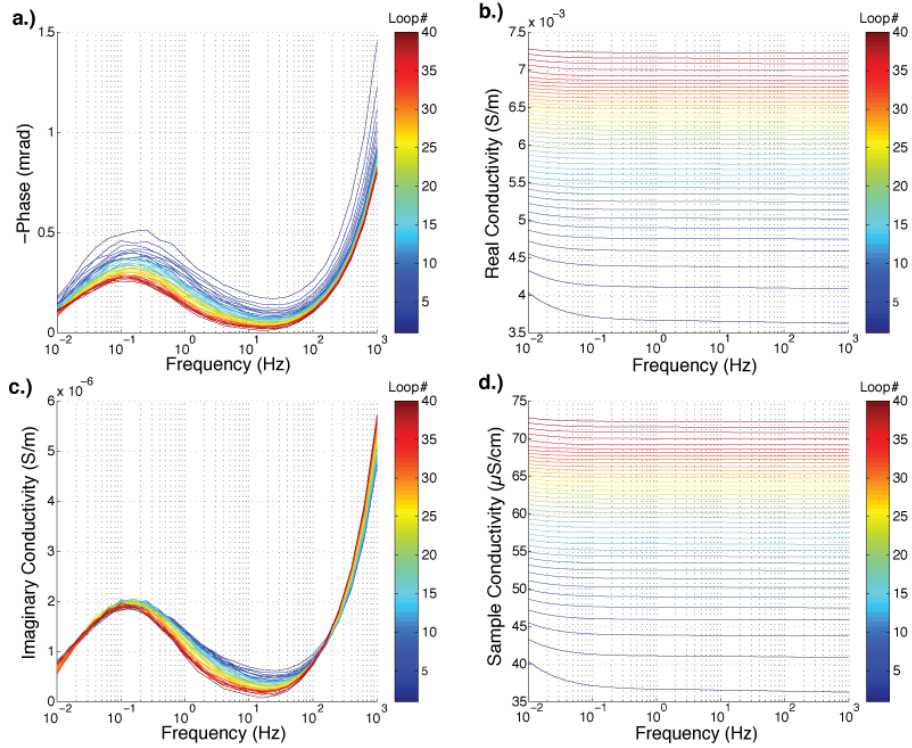


Figure 12: SIP response of 0.2-0.3 mm etching cream treated glass beads over 40 frequency sweeps from 1000 to 0.01 Hz with 26 log-spaced steps. a) phase in negative milliradians b) real component of the complex conductivity in S/m c) imaginary component of the complex conductivity in S/m and d) sample conductivity in $\mu\text{S/cm}$.

Immediately, we notice the constant increase in sample conductivity over time, which corresponds to a similar increase in the real component of the complex conductivity and a gradual diminishing of the phase response. Furthermore, the signals from the smallest glass bead size (Figure 10) are much cleaner than those from the largest bead size (Figure 12) most likely due to the higher signal in the smaller beads, which have a much higher surface area. As expected, the location of the phase peak decreases with increasing bead size as the lower frequencies polarize larger bead sizes. What is curious to note about the imaginary conductivity responses is that they appear to have a similar response at frequencies below the peak. Even though we see drastic changes in

the real conductivity and sample conductivity, the change in the imaginary conductivity is negligible.

Constant head permeability measurements were made on each column to measure both the influence of bead size and roughness and to compare to permeability results generated from NMR and SIP data. Figure 13 shows the average permeability of each replicate sample in each bead size and surface area treatment.

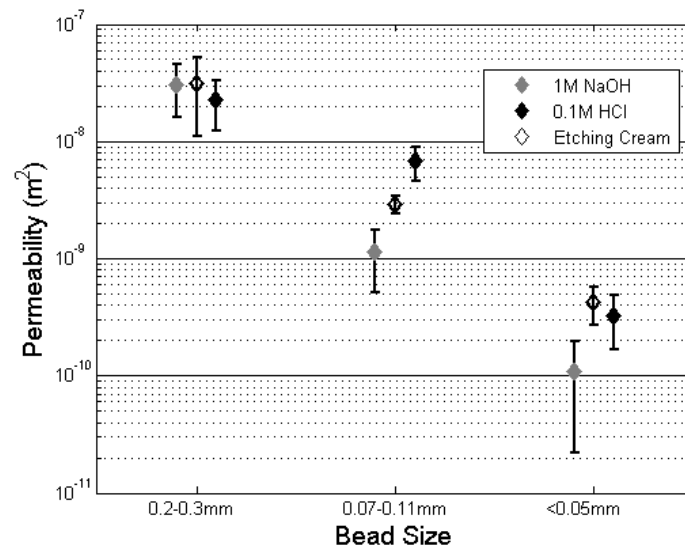


Figure 13: Average and standard deviation of permeability (m^2) as measured by the laboratory permeameter setup. Values are averages of three replicates for each bead size and treatment.

Generally, permeability increased with increasing grain size and decreased with increasing surface area, or grain roughness. Additionally, we see a smaller difference in permeability across surface area treatments in the largest bead size than the smaller bead sizes, most likely due to smaller surface area to volume ratios. Surface area treatments should have a much greater effect on smaller bead sizes because of the greater surface area available for etching.

DISCUSSION

In my research, I focus on relating NMR and SIP measured parameters, which are influenced by physical properties governing permeability. I start by discussing the effect of bead size and surface roughness on permeability. Next I examine the relationships between the NMR measured parameters and the permeability and the relationship between the SIP measured parameters and the permeability. Then, I consider the permeability predicted from either NMR or SIP alone and compare the results to the measured permeability. Finally, I consider potential routes for a combined NMR and SIP permeability relationship.

In theory, we would expect decreasing bead size and increasing surface roughness to decrease permeability. Decreasing the bead size reduces the hydraulic radii of pores, constricting pores and increasing resistance to flow. Decreasing bead size also increases S_{por} , which again increases resistance to flow through the increased friction force in the pore spaces. The permeability results in Figure 13 agree with this conclusion. Permeability consistently increases by about an order of magnitude with increasing bead size. Increasing surface roughness should exhibit a similar relationship. While increasing the bead roughness will not change the pore hydraulic radius, it will increase S_{por} without decreasing pore volume. This increased surface roughness per unit volume increases the friction applied to water flowing through the system, thereby decreasing permeability.

Returning to Figure 13, we do not observe as strong a relationship between permeability and surface roughness as we did with bead size. Only in the middle (0.07-0.11 mm) and smallest (<0.05 mm) bead sizes do we see a trend between roughness and permeability. In both the middle and smallest bead sizes, we see that the smoother acid

washed beads have a higher permeability than the base etched beads, which should have greater surface roughness and greater frictional resistance to flow. The etching cream results tended to be variable, most likely due to an error in experimental design. We might expect the etching cream treatment to etch the surface of the beads equal to or greater than the extent of the base treatment, and therefore have a similar permeability response. However, the etching cream treated beads have higher permeabilities than expected, especially with the smallest bead size. This could be due to the fact that residual cream may still have been attached to the bead, covering any surface area treatment that may have occurred and led to a smoother bead than expected. It must be noted that it is difficult to make any determination of bead roughness influence on permeability without BET surface area estimates or SEM bead images, which could not be obtained for this study.

There appears to be no observable difference in permeability between the three surface area treatments for the largest glass bead size. This could be due to the fact that these beads have the highest S_{por} , so that any surface area treatment will have less of an effect than they would on the smaller bead sizes with much higher S_{por} . With smaller changes in surface roughness, we would expect smaller influences of friction on water flow, leading to smaller changes on permeability. It appears that this insignificant change in surface roughness is the reason for the lack of variability between the permeabilities of the largest glass beads.

From the modified SDR equation (equation 6), we expect that the permeability will be a function of both the NMR relaxation time and the porosity. Figure 14a shows the plot of the measured permeability versus T_{2pk} . As expected, there appears to be a

strong correlation between permeability and T_{2pk} , with slower T_{2pk} corresponding to higher permeability and, likewise, faster T_{2pk} corresponding to lower permeability. Furthermore, for the smallest beads, the permeability decreases with T_{2pk} for each bead treatment; the acid washed beads with the smoothest expected surfaces have the highest permeability and the base etched beads with the roughest expected surface have the lowest permeability. The same trends are not observed for the largest glass beads. For these beads, the permeability does not change even though the surface treatments do not affect the value of T_{2pk} .

Figure 14b shows the plot of measured permeability versus the NMR measured porosity. This plot shows significant scatter and no firm conclusions can be made from this relationship. This is likely because porosity does not vary as widely with most unconsolidated sediments as it does with consolidated sediments. Changes in porosity are expected to have a minimal influence on the permeability of the glass bead system compared to changes in r_h , S_{por} , and surface roughness. The SDR equation (equation 5) was originally formulated for consolidated sediments with greater variation in porosity.

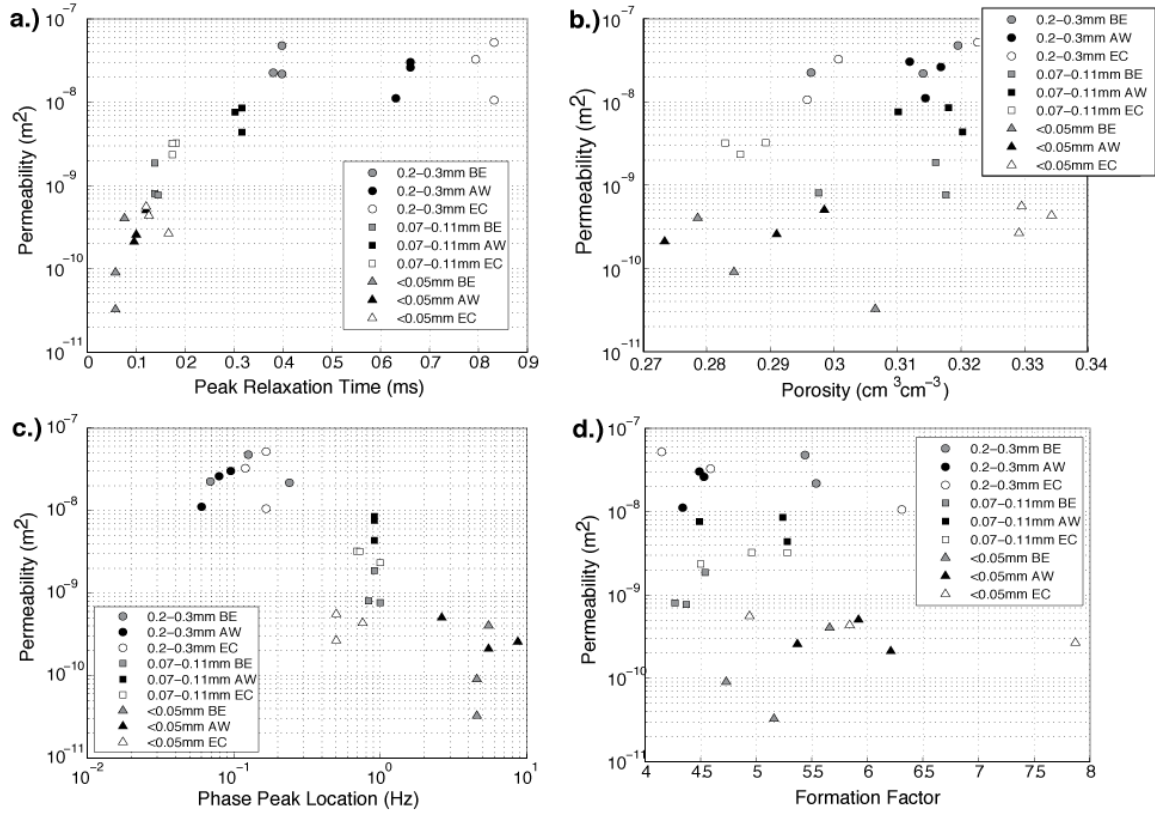


Figure 14: NMR and SIP parameter relationships with permeability a) permeameter measured permeability vs. peak T_2 relaxation time in milliseconds for each replicate sample b) permeameter measured permeability vs. NMR measured porosity c) permeameter measured permeability vs. SIP phase peak location in Hz d) permeameter measured permeability versus formation factor.

We next consider the relationship between SIP measured parameters and permeability. The Revil and Florsch (2010) model (equation 12) tells us that the permeability is a function of both the phase peak location and the formation factor. Figure 14c shows permeability plotted versus the phase peak location in. As phase peaks at higher frequencies would indicate smaller bead sizes, and peaks at lower frequencies would indicate larger bead sizes, we would expect to see an inverse relationship between permeability and phase peak location, which is clearly demonstrated in Figure 14c. However, while the relationship between bead size, permeability, and phase peak may be

clear, we do not observe any difference in the phase peak location due to a change in the surface roughness, suggesting that the SIP measurements are not sensitive to surface roughness.

Finally, we observe the relationship between permeability and formation factor (Figure 14d). As the formation factor describes the electrical connectivity of the measured system, I would expect it to relate to the hydraulic connectivity and permeability of the system as well. However, I do not observe this relationship in my data, possibly due to two reasons. First, the estimate of formation factor in this study was hindered by bead leaching and was only made at two relatively low fluid conductivities. Second, formation factors, as with porosities, do not vary much within these samples (as expected for unconsolidated sediments).

Next we compare the measured permeability to the permeability predicted from NMR parameters (using equation 6; Figure 15). The SDR equation provides a decent relationship between the estimated and measured permeability. This is most likely due to the strong relationship shown before between T_2 peak location and permeability. The T_2 relaxation distribution is representative of the pore size distribution of a sample, with the peak location representing the dominant pore size. However, it has been shown that NMR signals are influenced by increases in grain surface roughness as well. The question is whether surface roughness influences permeability as well. To the author's knowledge, no research has defined a relationship between the surface roughness of unconsolidated material and permeability. However, research on the permeability of fractured rock has proven a relationship between permeability and surface roughness in fractures, dependant on the ratios of surface roughness to aperture size (Thompson and

Brown, 1991; Or and Teller, 2000). Theoretically, an inverse relationship should exist between grain surface roughness and permeability. With increasing surface roughness, friction and surface area available for adhesion of water should increase, thereby slowing the flow of water through a porous system. In my data, as demonstrated in Figure 13, I observe only a small dependence of permeability on surface roughness for the small and medium glass beads and no dependence for the large glass beads. This weak relationship could be a potential source of error for the NMR permeability estimate. I observe a distinct effect of surface roughness on NMR measurements, but the relationship between surface roughness and permeability is much less clear.

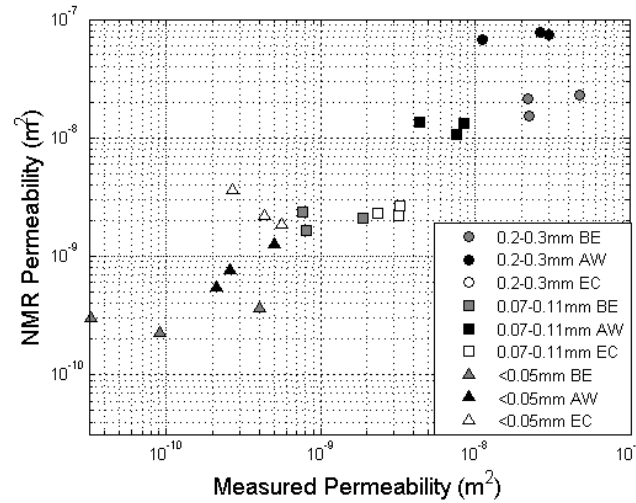


Figure 15: NMR estimated permeability using the SDR equation versus negative log laboratory permeameter measured permeability. SDR parameter $a = 1\text{E-}6$. RMSE = 1.97×10^{-8} ; $R^2 = 0.7836$

Next we compare the measured permeability to the permeability predicted from SIP parameters (using equation 12; Figure 16). The SIP measured parameters were utilized to estimate permeability based solely on the one method. However, as the NMR relaxation time, the SIP relaxation time τ can be influenced by other non-geometric factors such as variable or unknown pore fluid conductivity. Modifying Revil and

Florsch's (2010) equation, I use a peak value for τ that better defines my columns with distinct bead sizes as opposed to samples with a greater grain size distribution where a mean τ value would be more appropriate.

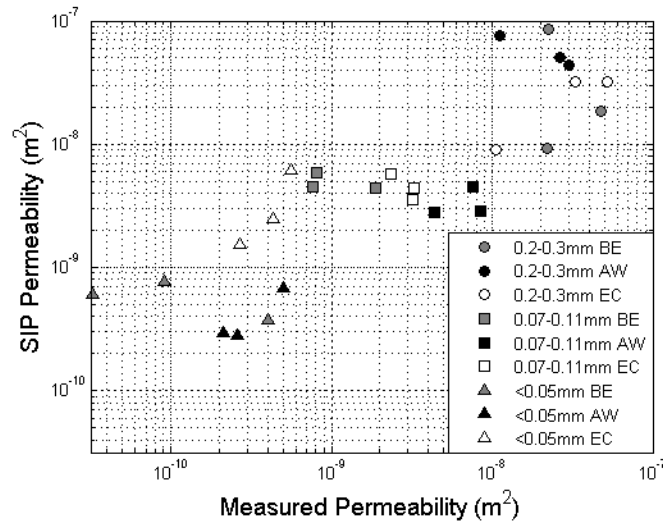


Figure 16: SIP estimated permeability using equation 12 versus the laboratory permeameter measured permeability. RMSE = 1.64×10^{-8} ; $R^2 = 0.4871$

While the SIP measured permeability does not match the true permeability as well as NMR, it does provide a decent estimate (Figure 16). This could be one reason for the smaller correlation and higher RMSE associated with the SIP permeability method over the NMR method. In addition, the issue of bead dissolution almost certainly led to increased error in SIP measurements, carrying over to permeability estimates as well. However, both methods performed remarkably well with near identical root mean square error (RMSE) and decent correlation coefficient (R^2). Most importantly, both methods generally follow a 1:1 trend line, indicating that the models exhibited a strong relationship to the true permeability and that there is no general bias in the data.

A mechanistic approach was taken during formulation of a combined permeability model. I return to Katz and Thompson's (1986) permeability relationship, which

describes the square of a length scale over tortuosity and multiplied by a fitting parameter (equation 11). As I do not have any other measures of tortuosity, the formation factor will take its place as in the SIP model. Despite the issues associated with its estimation in this research, the correlation shown between formation factor and porosity in equation 10 should be enough to justify its use in a combined model. For the length scale, I look to NMR parameters. As stated above, permeability should theoretically depend on surface roughness. Therefore, when I look to define the length scale in equation 11, the T_2 peak relaxation time makes logical sense as it not only defines the dominant pore size, but it is also influenced by varying surface roughness (Figure 4). Figure 13 and the SDR equation results, however, suggest that the NMR results are more sensitive to changes in surface area than permeability. Instead of T_{2pk} defining the length scale on its own, it may be best to mitigate the effects of surface roughness with a measurement less sensitive to changes in bead roughness. The peak SIP relaxation time, converted to peak grain size d_{pk} (equation 14), should provide a reasonable representation of the dominant pore space without a strong influence from bead surface roughness. By multiplying the d_{pk} by T_{2pk} instead of taking a length scale squared, we might be able to account for a length scale that is only slightly influenced by surface roughness while incorporating both NMR and SIP measured parameters.

Placing these values into equation 11, we obtain an equation for estimating permeability based on combined NMR and SIP parameters:

$$k = a \frac{T_{2pk}^{-2} d_{pk}}{F} \quad (15)$$

where a is an empirical fitting parameter. While a mechanistic approach was taken to design this equation, the use of an empirical fitting parameter means that it is not entirely mechanistic. Figure 17 shows the results of this method of permeability estimation.

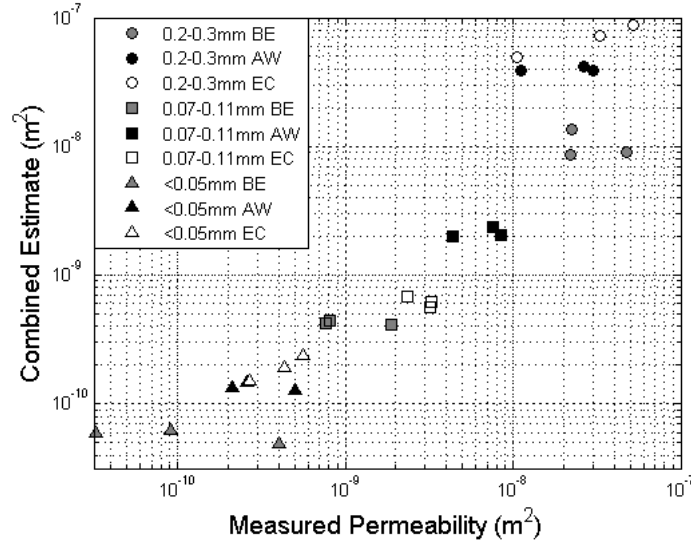


Figure 17: Combined permeability model estimates versus laboratory permeameter measured permeability. $a = 5E-6$. $RMSE = 1.10 \times 10^{-8}$; $R^2 = 0.7836$

The R^2 value for the combined model is higher than the SIP model, meaning there is greater linearity among the data, and the RMSE is slightly lower than both the NMR and SIP models. This slight increase in accuracy and reliability could be attributed to the inclusion of both NMR and SIP data for length scale measurements. SIP is sensitive to the connectivity of the pore spaces and grain size, which influence tortuosity and r_h . SIP does not appear to be sensitive to surface roughness (Figure 14c), which was shown to have a small but tangible effect on permeability (Figure 13). NMR is sensitive to these changes in surface roughness, but it may be overestimating its significance in permeability estimation through the SDR equation (Figure 14a). Therefore, by combining these two parameters, we account for more of the pore scale properties that are influencing these glass bead packs.

Given the problematic experiment design and materials, moderately accurate permeability results were obtained by combining the NMR and SIP data. By combining the data, the overdependence of T_{2pk} on surface roughness was mitigated by the less sensitive d_{pk} . When SIP signals and F estimates are perturbed by fluctuating or unknown pore fluid conductivity, they are mitigated by NMR data insensitive to these issues.

CONCLUSION

Geophysical surveys are valuable tools in the fields of water resources and environmental science due to their decreased sampling time, cost, and invasiveness as compared to traditional sampling methods. Unfortunately, indirect measurements of permeability may be influenced by unrealistic signal responses due to pore scale properties such as fluctuating pore fluid conductivity or increased surface roughness. The variety of glass bead packs used in this experiment highlight some of the situations in which SIP and NMR permeability methods may break down. Bead dissolution led to fluctuating pore fluid conductivity in the glass bead packs that greatly interfered with the SIP signal. Increased surface roughness on the glass beads led to significantly altered NMR results, but only minimally altered permeability.

While the new combined model may not perform significantly better than the existing models in this situation, its slight increase in reliability and accuracy highlights the benefits of combining the methods' parameters. By dividing the length scale of our permeability equation into NMR and SIP estimated parameters, we allow one parameter to mitigate any negative effects the other might have. For example, in this experiment, the fluctuating pore fluid conductivity led to problematic SIP results, which was not an

issue with NMR because it is not sensitive to fluid conductivity. On the other hand, NMR data was influenced by changes in surface area that minimally influenced permeability, and only at smaller bead sizes. Surface roughness did not appear to influence SIP data, which might have mitigated this effect in NMR data.

Therefore, while the combined permeability method did not provide more accurate estimates of permeability, it may be useful in more situations than either method alone. Additionally, this research highlights the fact that geophysical measurements are useful in identifying which pore scale properties have a greater influence on permeability. In the glass bead packs, S_{por} and r_h were found to be the dominant factors influencing permeability. NMR identified large suspected changes in surface roughness, but these changes appeared to have a minimal effect on permeability. SIP measurements appeared to be insensitive to surface roughness, yet I was still able to obtain permeability estimates from SIP data with similar error and correlation to NMR permeability estimates. Both methods were highly sensitive to changes in S_{por} and r_h with changing bead sizes, which led to their reasonable and moderately accurate results. The usefulness in identifying pertinent pore scale properties through these two geophysical methods emphasizes the benefit of combining their measurements for a more accurate, robust, and relevant permeability model.

REFERENCES

- Archie, G.E., 1942. The electrical resistivity log as an aid in determining some reservoir characteristics. *Petroleum Transactions of AIME* 146, 54–62.
- Aster, R., Borchers, B., Thurber, C.H., 2013. *Parameter estimation and inverse problems* (2nd ed.). Waltham, MA: Academic Press.
- Bryar, T.R., Knight, R.J., 2003. Laboratory studies of the effect of sorbed oil on proton nuclear magnetic resonance. *Geophysics* 68, 942–948.
- Cassiani, G., Kemna, A., Villa, A., Zimmermann, E., 2009. Spectral induced polarization for the characterization of free-phase hydrocarbon contamination of sediments with low clay content. *Near Surf. Geophys.* 547–562.
- Coates, G. R., L. Xiao, and M. G. Prammer, 1999. *NMR logging principles and applications*: Halliburton Energy Services, Houston.
- Dlubac, K., Knight, R., Keating, K., 2014. A numerical study of the relationship between NMR relaxation and permeability in sands and gravels. *Near Surf. Geophys.* 12, 219–230.
- Doremus, R.H., 1975. Interdiffusion of hydrogen and alkali ions in a glass surface. *Journal of Non-Crystalline Solids*. 19, 137–144.
- Irons, T., Martin, K., Finn, C., Bloss, B., Horton, R., 2014. Using Nuclear Magnetic Resonance and Transient Electromagnetics to characterise water distribution beneath an ice covered volcanic crater: the case of Sherman Crater Mt. Baker, Washington. *Near Surf. Geophys.* 12, 285–296.
- Katz, A., Thompson, A., 1986. Quantitative prediction of permeability in porous rock. *Phys. Rev. B. Physical Review B*. 34, 8179–8181.
- Keating, K., 2014. A laboratory study to determine the effect of surface area and bead diameter on NMR relaxation rates of glass bead packs. *Near Surf. Geophys.* 1–12.
- Keating, K., Knight, R., 2007. A laboratory study to determine the effect of iron oxides on proton NMR measurements. *Geophysics* 72, E27–E32.
- Keating, K., Knight, R., 2010. A laboratory study of the effect of Fe(II)-bearing minerals on nuclear magnetic resonance (NMR) relaxation measurements. *Geophysics* 75, F71–F82.
- Lanford, W., Davis, K., Laursen, T., Groleau, R., Doremus, R.H., 1979. Hydration of soda-lime glass. *Journal of Non-Crystalline Solids* 33, 249–266.
- Leroy, P., Revil, a, Kemna, a, Cosenza, P., Ghorbani, a, 2008. Complex conductivity of water-saturated packs of glass beads. *J. Colloid Interface Sci.* 321, 103–117.
- Lesmes, P., Frye, M., 2001. Influence of pore fluid chemistry on the complex conductivity and induced polarization responses of Berea sandstone. *J. Geophys. Res.* 106, 4079–4090.
- Or, D., Tuller, M., 2000. Flow in unsaturated fractured porous media: Hydraulic conductivity of rough surfaces. *Water Resour. Res.* 36, 1165–1177.
- Paterson, M.S. 1983. The equivalent channel model for permeability and resistivity in fluid-saturated rock—A re-appraisal. *Mech. Mater.* 2 (4): 345–352.
- Pederson, L.R., Baer, D.R., McVay, G.L., Engelhard, M.H., 1986. Reaction of soda lime silicate glass in isotopically labelled water. *Journal of Non-Crystalline Solids* 86, 369–380.

- Revil, a., Florsch, N., 2010. Determination of permeability from spectral induced polarization in granular media. *Geophys. J. Int.* 1480–1498.
- Schmutz, M., Revil, a., Vaudelet, P., Batzle, M., Viñao, P.F., Werkema, D.D., 2010. Influence of oil saturation upon spectral induced polarization of oil-bearing sands. *Geophys. J. Int.* 183, 211–224.
- Simpson, J.H., Carr, H.Y., 1958. Diffusion and nuclear spin relaxation in water. *The Physical Review*, 111, 1201-1202.
- Slater, L., 2007. Near surface electrical characterization of hydraulic conductivity: from petrophysical properties to aquifer geometries—a review. *Surv. Geophys.* 28, 169–197.
- Thompson, M.E., Brown, S.R., 1991. The effect of anisotropic surface roughness on flow and transport in fractures. *Journal of Geophysical Research: Solid Earth*, 96, 21923-21932.
- Walsh, J.B. and Brace, W.F. 1984. The effect of pressure on porosity and the transport properties of rock. *Journal of Geophysical Research: Solid Earth* 89 (B11): 9425-9431.
- Walsh, D.O., Grunewald, E.D., Turner, P., Hinnell, A., Ferre, T.P.A., 2014. Surface NMR instrumentation and methods for detecting and characterizing water in the vadose zone. *Near Surf. Geophys.* 1–14.
- Waxman, M.H., Smits, L.J.M., 1968. Electrical Conductivities in Oil-Bearing Shaly Sands. *Society of Petroleum Engineers Journal*, 243, 107-122.
- Weller, A., Nordsiek, S., Debschütz, W., 2010. Estimating permeability of sandstone samples by nuclear magnetic resonance and spectral-induced polarization. *Geophysics* 75, E215–E226.
- Zengin, H., Hu, B., Siddiqui, J.A., Ottenbrite, R.M., 2006. Surface modification of glass beads with poly (acrylic acid). *Polym. Adv. Technol.* 17, 372–378.
- Zisser, N., Kemna, A., Nover, G., 2010. Relationship between low-frequency electrical properties and hydraulic permeability of low-permeability sandstones. *Geophysics* 75, E131–E141.

APPENDIX A

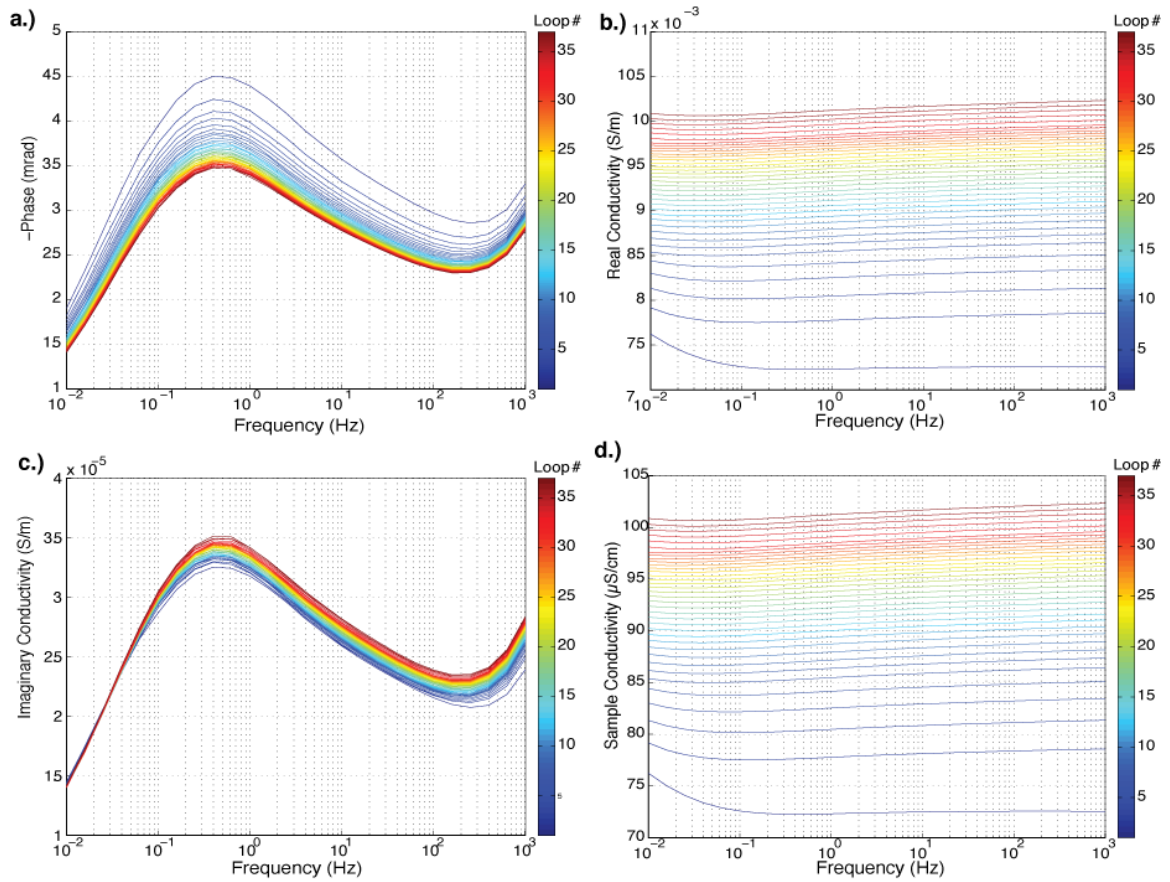


Figure A1: SIP response of <0.05 mm etching cream treated glass beads, sample 1, over 40 frequency sweeps from 1000 to 0.01 Hz with 26 log-spaced steps. a) phase in negative milliradians b) real component of the complex conductivity in S/m c) imaginary component of the complex conductivity in S/m and d) sample conductivity in μ S/cm.

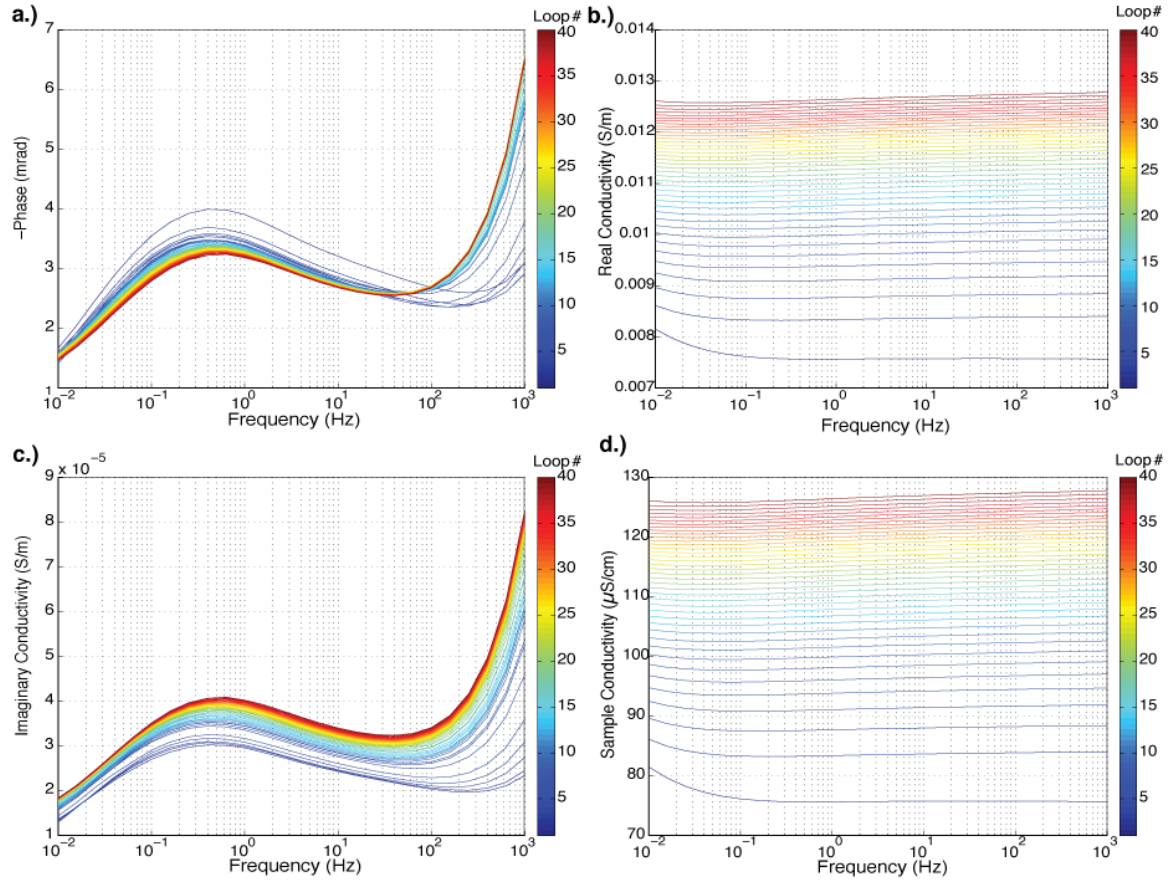


Figure A2: SIP response of <0.05 mm etching cream treated glass beads, sample 2, over 40 frequency sweeps from 1000 to 0.01 Hz with 26 log-spaced steps. a) phase in negative milliradians b) real component of the complex conductivity in S/m c) imaginary component of the complex conductivity in S/m and d) sample conductivity in μ S/cm.

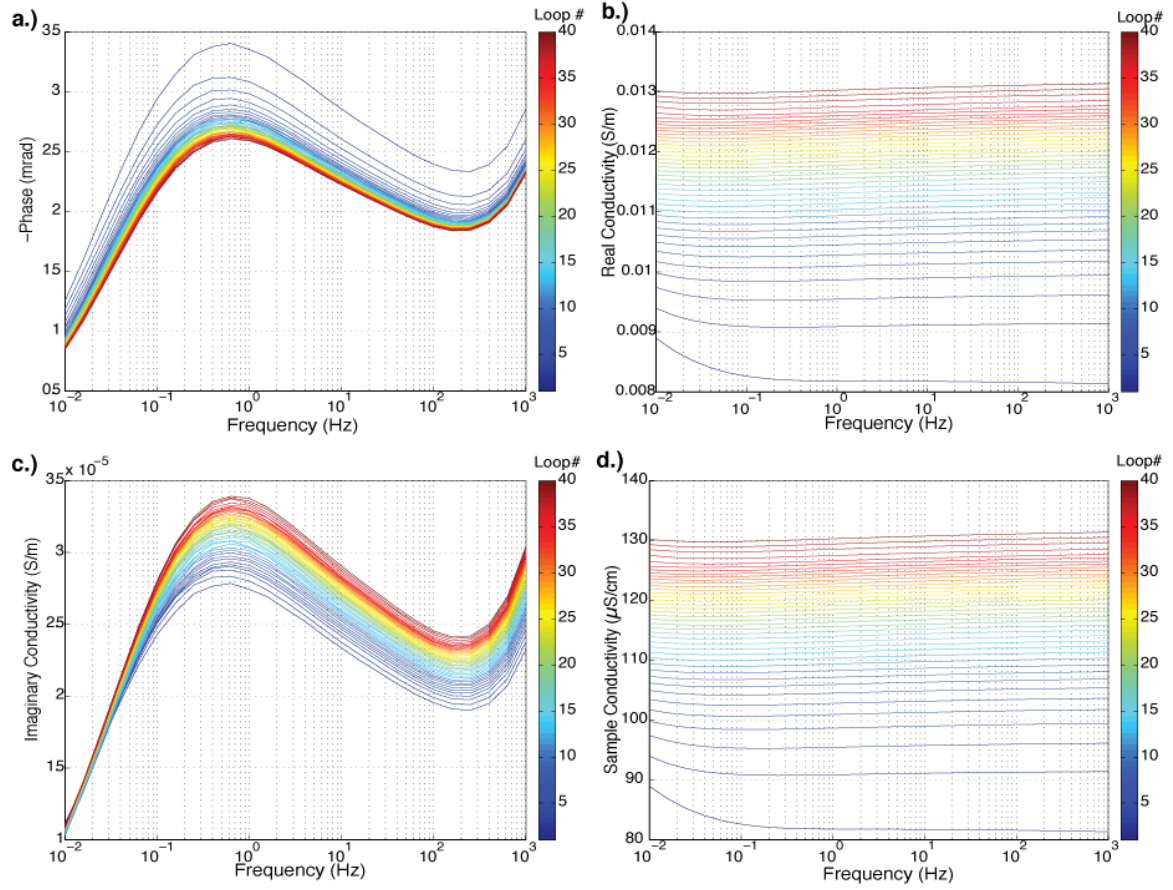


Figure A3: SIP response of <0.05 mm etching cream treated glass beads, sample 3, over 40 frequency sweeps from 1000 to 0.01 Hz with 26 log-spaced steps. a) phase in negative milliradians b) real component of the complex conductivity in S/m c) imaginary component of the complex conductivity in S/m and d) sample conductivity in μ S/cm.

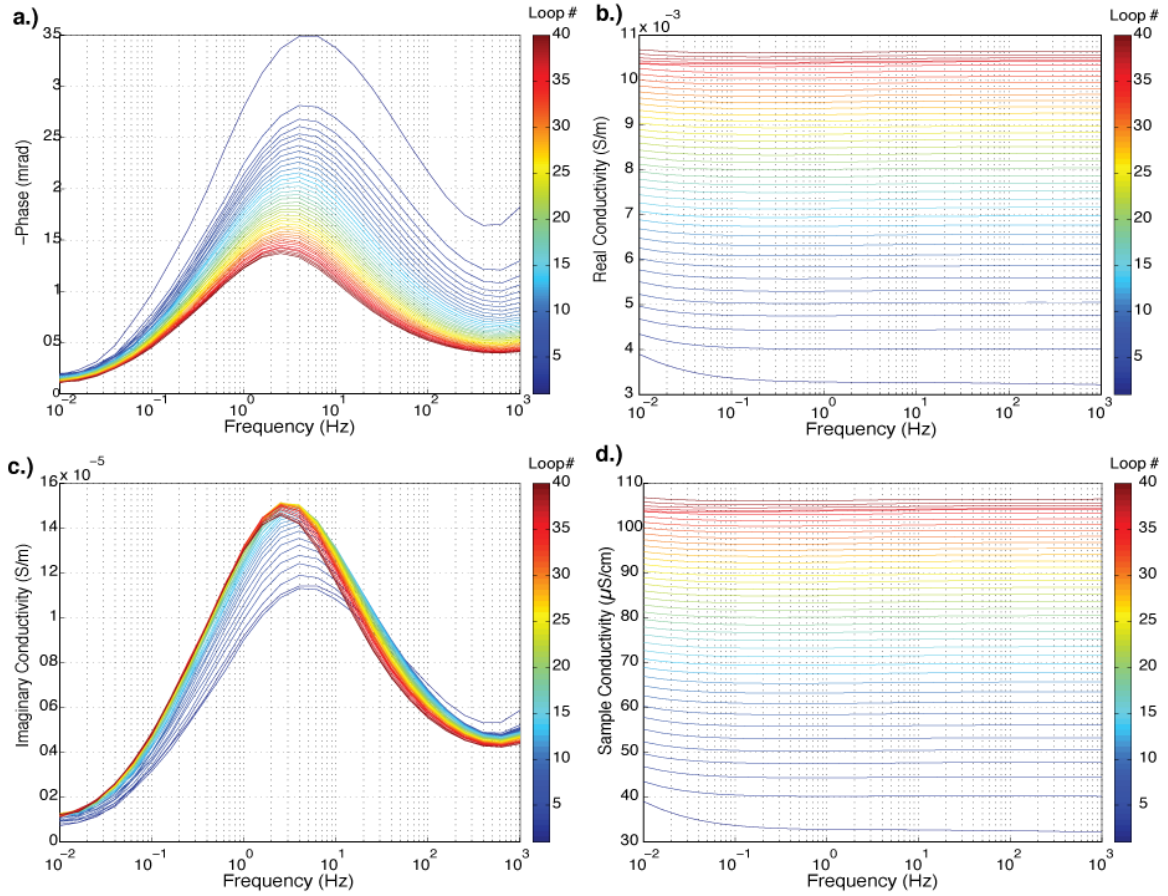


Figure A4: SIP response of <0.05 mm 0.1 M HCl treated glass beads, sample 1, over 40 frequency sweeps from 1000 to 0.01 Hz with 26 log-spaced steps. a) phase in negative milliradians b) real component of the complex conductivity in S/m c) imaginary component of the complex conductivity in S/m and d) sample conductivity in $\mu\text{S/cm}$.

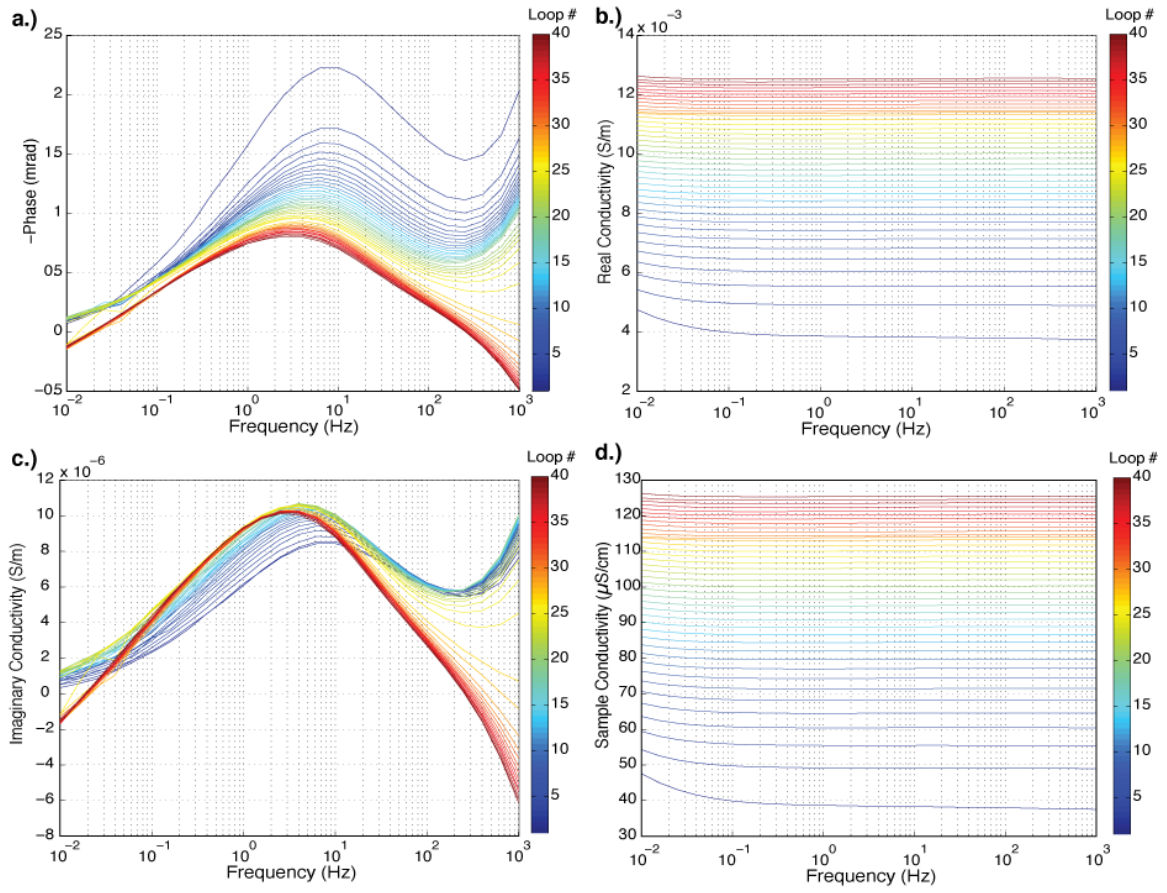


Figure A5: SIP response of <0.05 mm 0.1 M HCl treated glass beads, sample 2, over 40 frequency sweeps from 1000 to 0.01 Hz with 26 log-spaced steps. a) phase in negative milliradians b) real component of the complex conductivity in S/m c) imaginary component of the complex conductivity in S/m and d) sample conductivity in $\mu\text{S/cm}$.

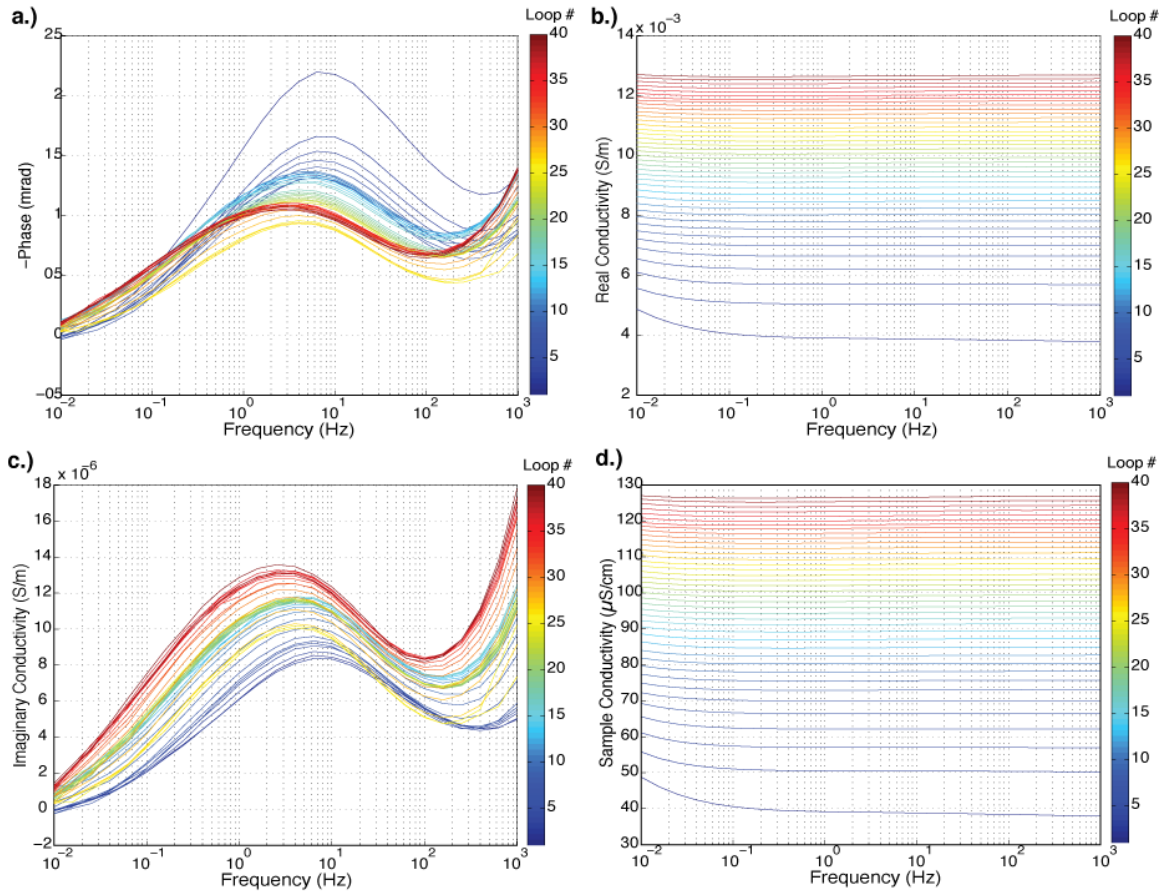


Figure A6: SIP response of <0.05 mm 0.1 M HCl treated glass beads, sample 3, over 40 frequency sweeps from 1000 to 0.01 Hz with 26 log-spaced steps. a) phase in negative milliradians b) real component of the complex conductivity in S/m c) imaginary component of the complex conductivity in S/m and d) sample conductivity in $\mu\text{S/cm}$.

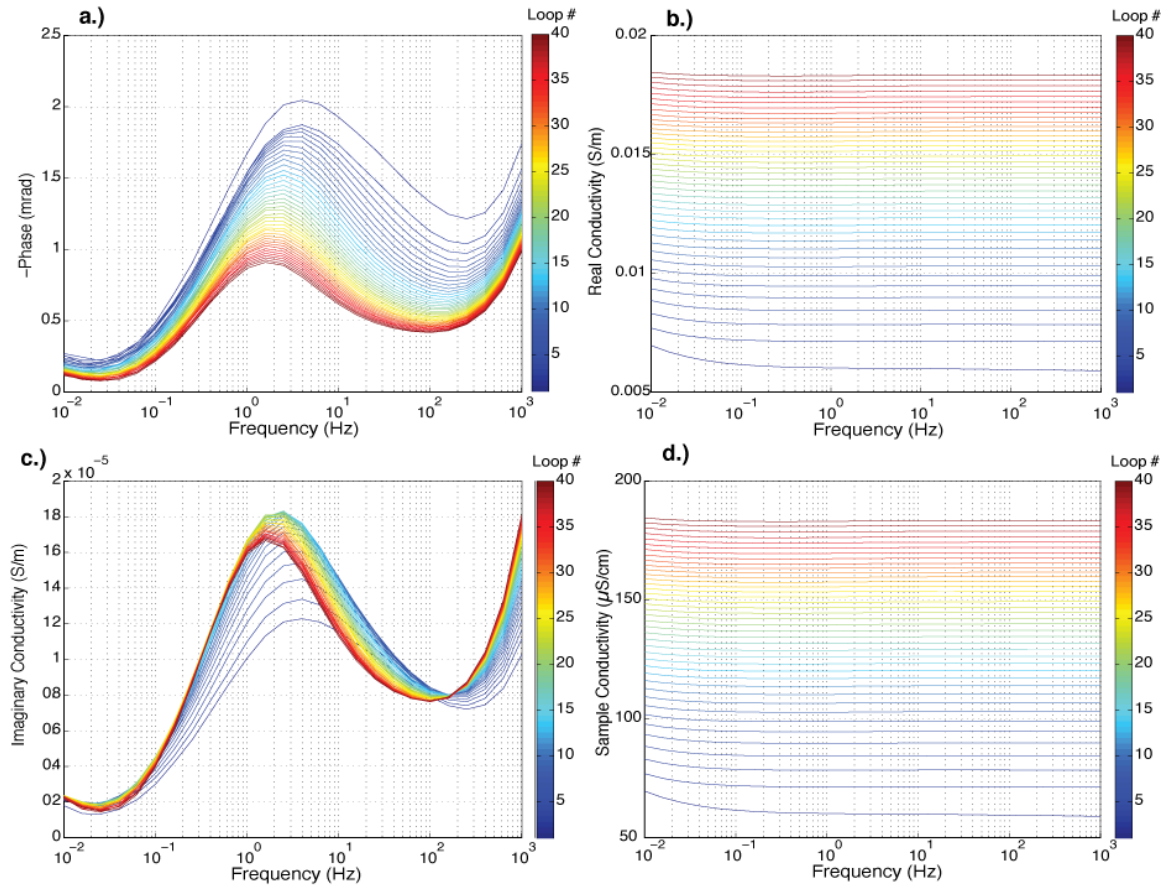


Figure A7: SIP response of <0.05 mm 1 M NaOH treated glass beads, sample 1, over 40 frequency sweeps from 1000 to 0.01 Hz with 26 log-spaced steps. a) phase in negative milliradians b) real component of the complex conductivity in S/m c) imaginary component of the complex conductivity in S/m and d) sample conductivity in $\mu\text{S/cm}$.

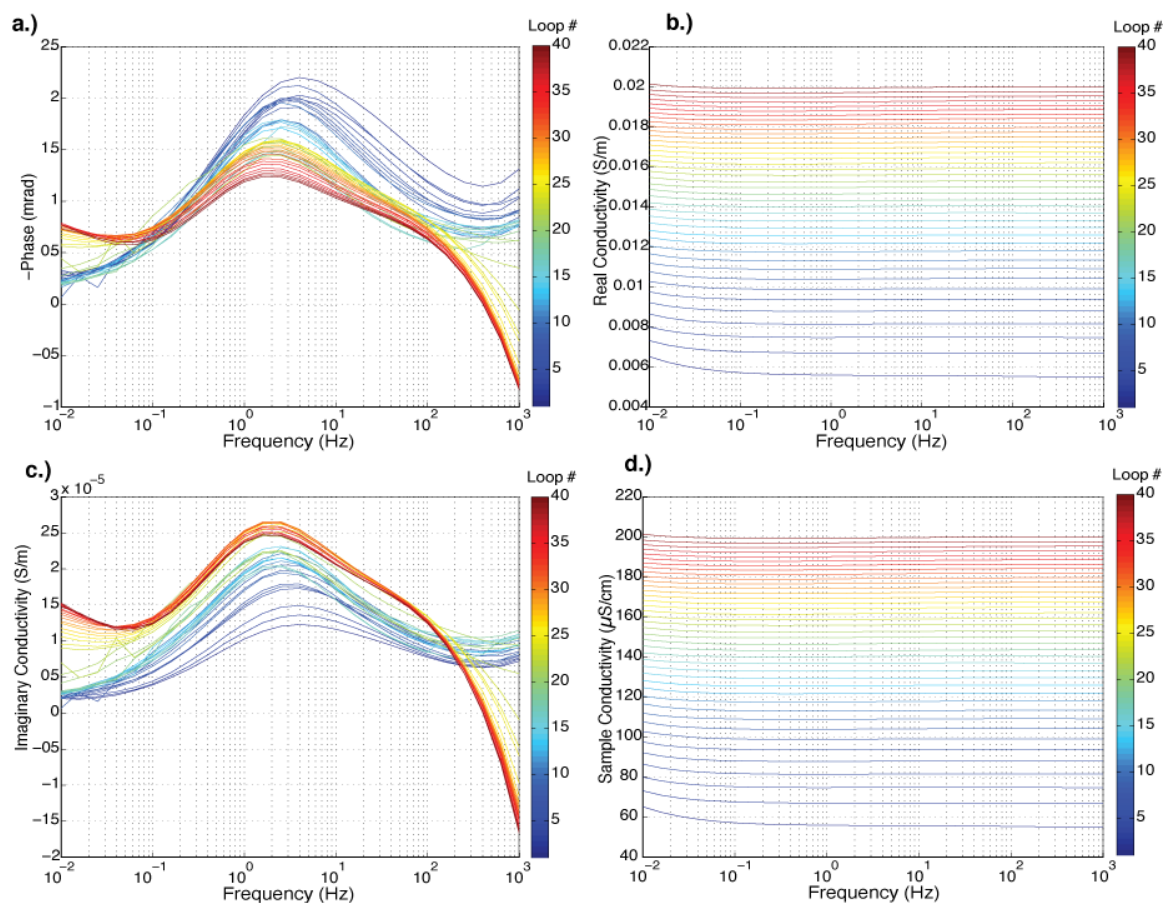


Figure A8: SIP response of <0.05 mm 1 M NaOH treated glass beads, sample 2, over 40 frequency sweeps from 1000 to 0.01 Hz with 26 log-spaced steps. a) phase in negative milliradians b) real component of the complex conductivity in S/m c) imaginary component of the complex conductivity in S/m and d) sample conductivity in $\mu\text{S/cm}$.

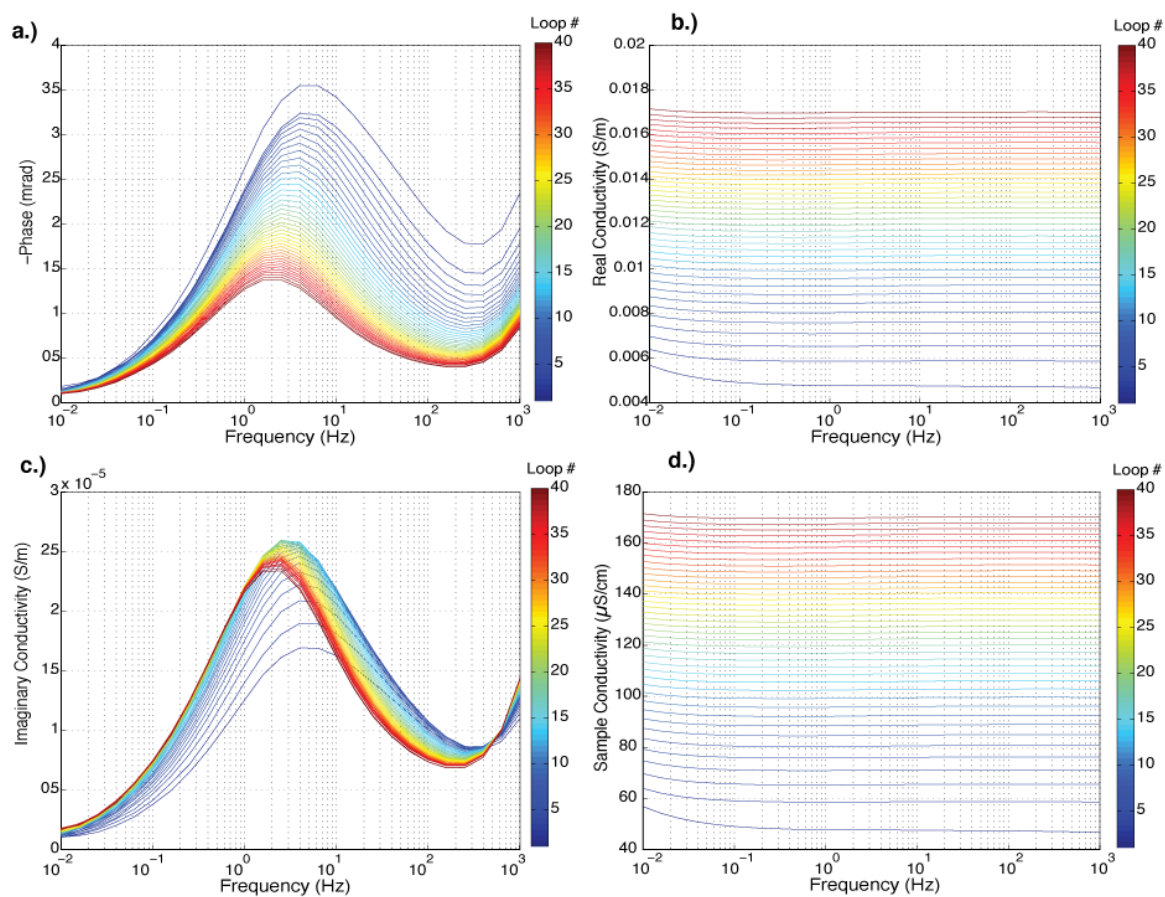


Figure A9: SIP response of <0.05 mm 1 M NaOH treated glass beads, sample 2, over 40 frequency sweeps from 1000 to 0.01 Hz with 26 log-spaced steps. a) phase in negative milliradians b) real component of the complex conductivity in S/m c) imaginary component of the complex conductivity in S/m and d) sample conductivity in $\mu\text{S/cm}$.

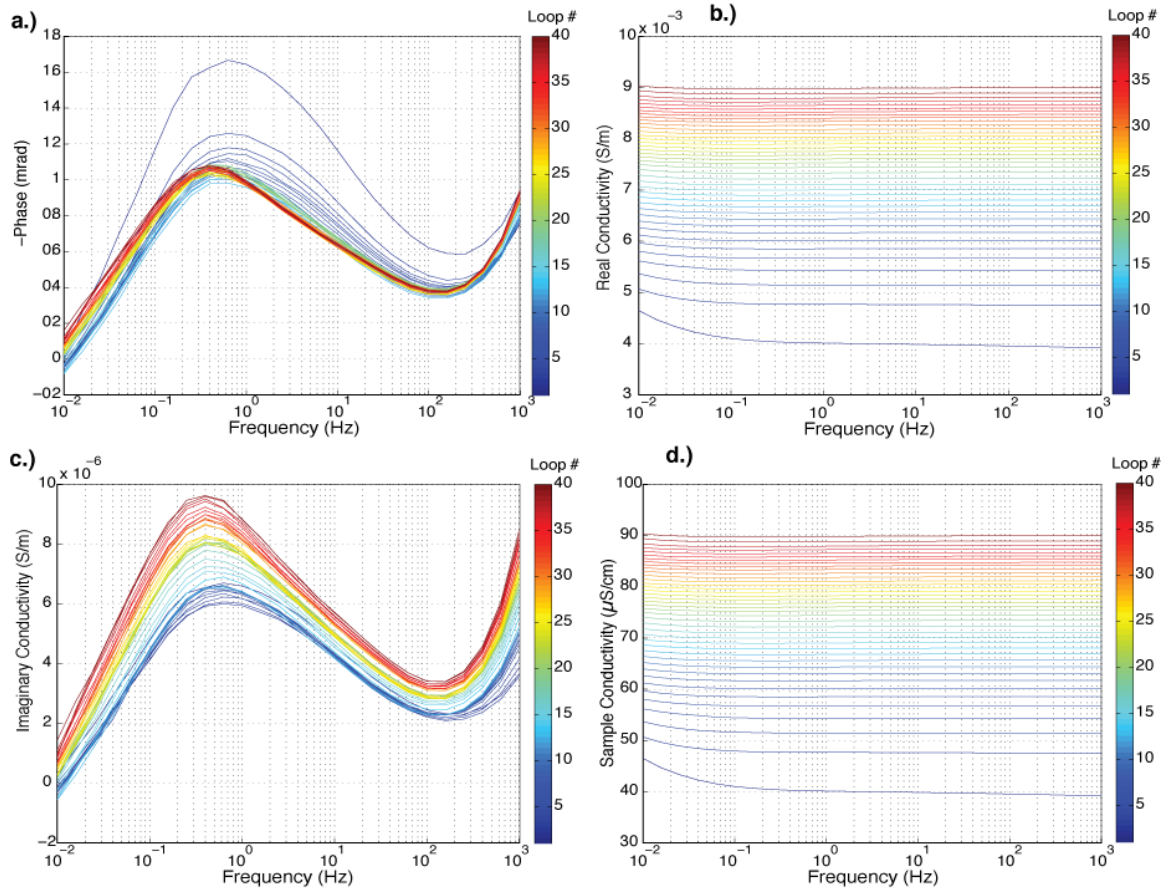


Figure A10: SIP response of 0.07-0.11 mm etching cream treated glass beads, sample 1, over 40 frequency sweeps from 1000 to 0.01 Hz with 26 log-spaced steps. a) phase in negative milliradians b) real component of the complex conductivity in S/m c) imaginary component of the complex conductivity in S/m and d) sample conductivity in $\mu\text{S/cm}$.

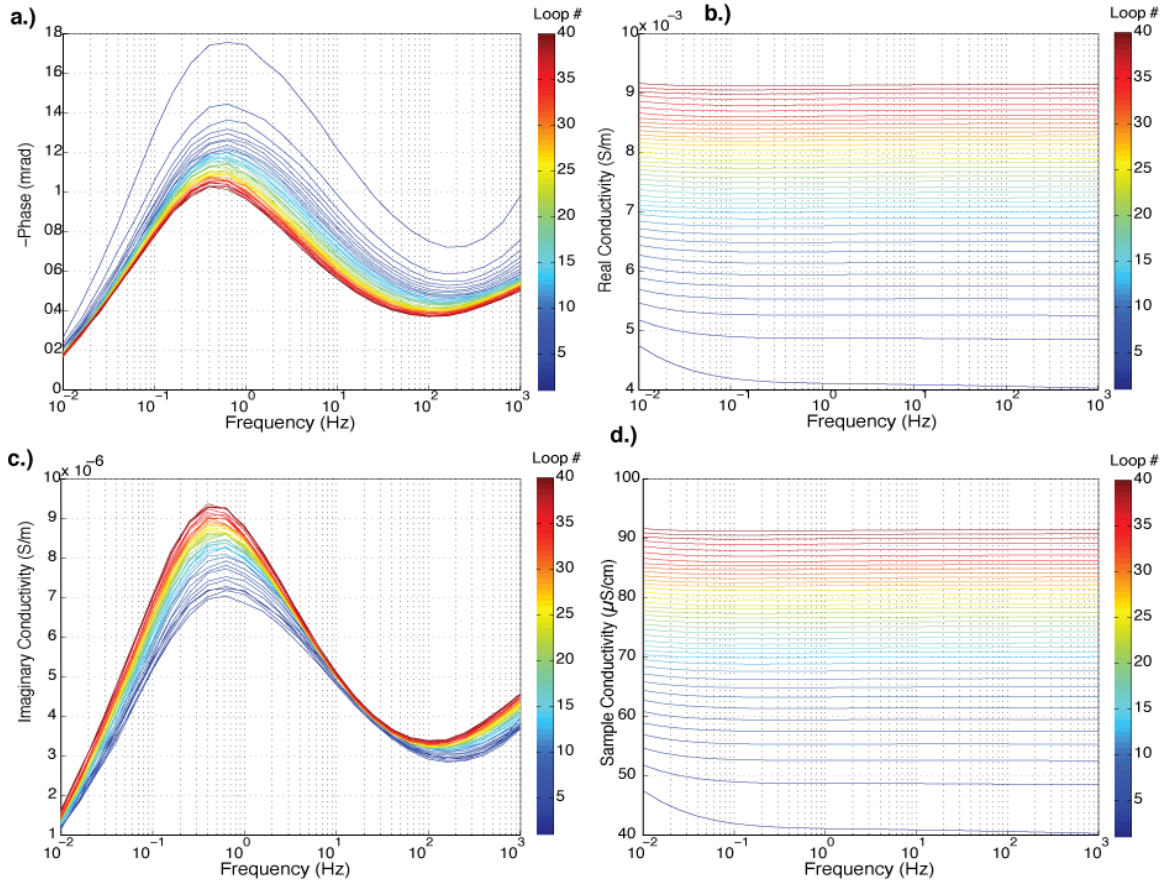


Figure A11: SIP response of 0.07-0.11 mm etching cream treated glass beads, sample 2, over 40 frequency sweeps from 1000 to 0.01 Hz with 26 log-spaced steps. a) phase in negative milliradians b) real component of the complex conductivity in S/m c) imaginary component of the complex conductivity in S/m and d) sample conductivity in $\mu\text{S/cm}$.

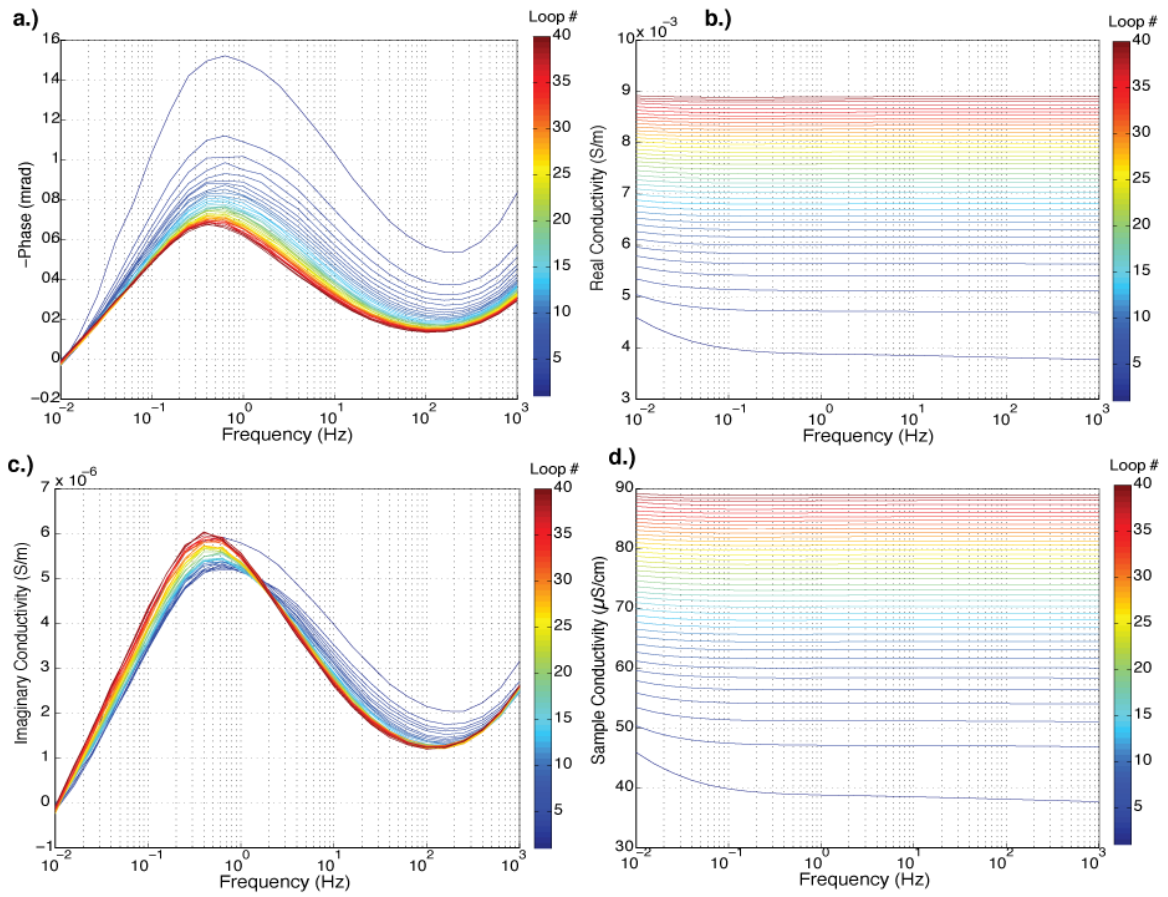


Figure A12: SIP response of 0.07-0.11 mm etching cream treated glass beads, sample 3, over 40 frequency sweeps from 1000 to 0.01 Hz with 26 log-spaced steps. a) phase in negative milliradians b) real component of the complex conductivity in S/m c) imaginary component of the complex conductivity in S/m and d) sample conductivity in $\mu\text{S/cm}$.

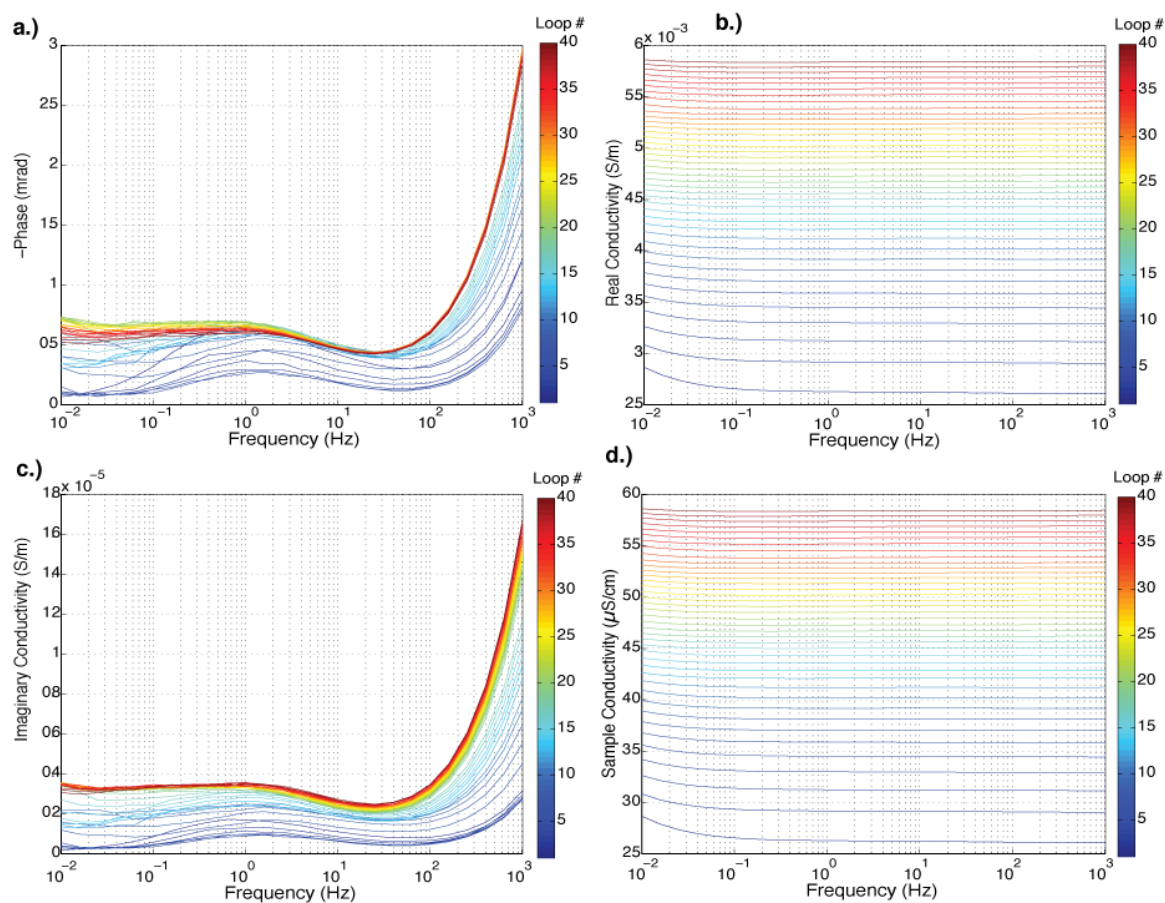


Figure A13: SIP response of 0.07-0.11 mm 0.1 M HCl treated glass beads, sample 1, over 40 frequency sweeps from 1000 to 0.01 Hz with 26 log-spaced steps. a) phase in negative milliradians b) real component of the complex conductivity in S/m c) imaginary component of the complex conductivity in S/m and d) sample conductivity in $\mu\text{S/cm}$.

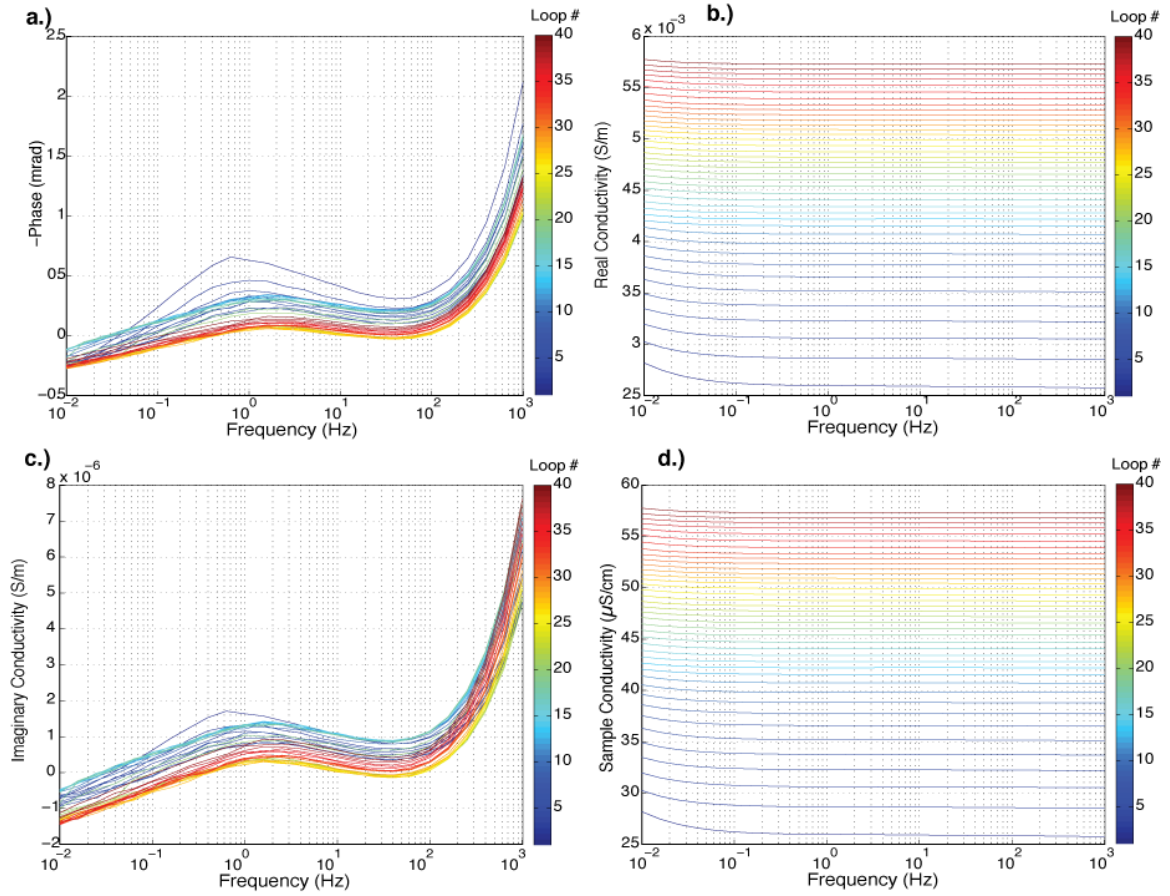


Figure A14: SIP response of 0.07-0.11 mm 0.1 M HCl treated glass beads, sample 2, over 40 frequency sweeps from 1000 to 0.01 Hz with 26 log-spaced steps. a) phase in negative milliradians b) real component of the complex conductivity in S/m c) imaginary component of the complex conductivity in S/m and d) sample conductivity in $\mu\text{S/cm}$.

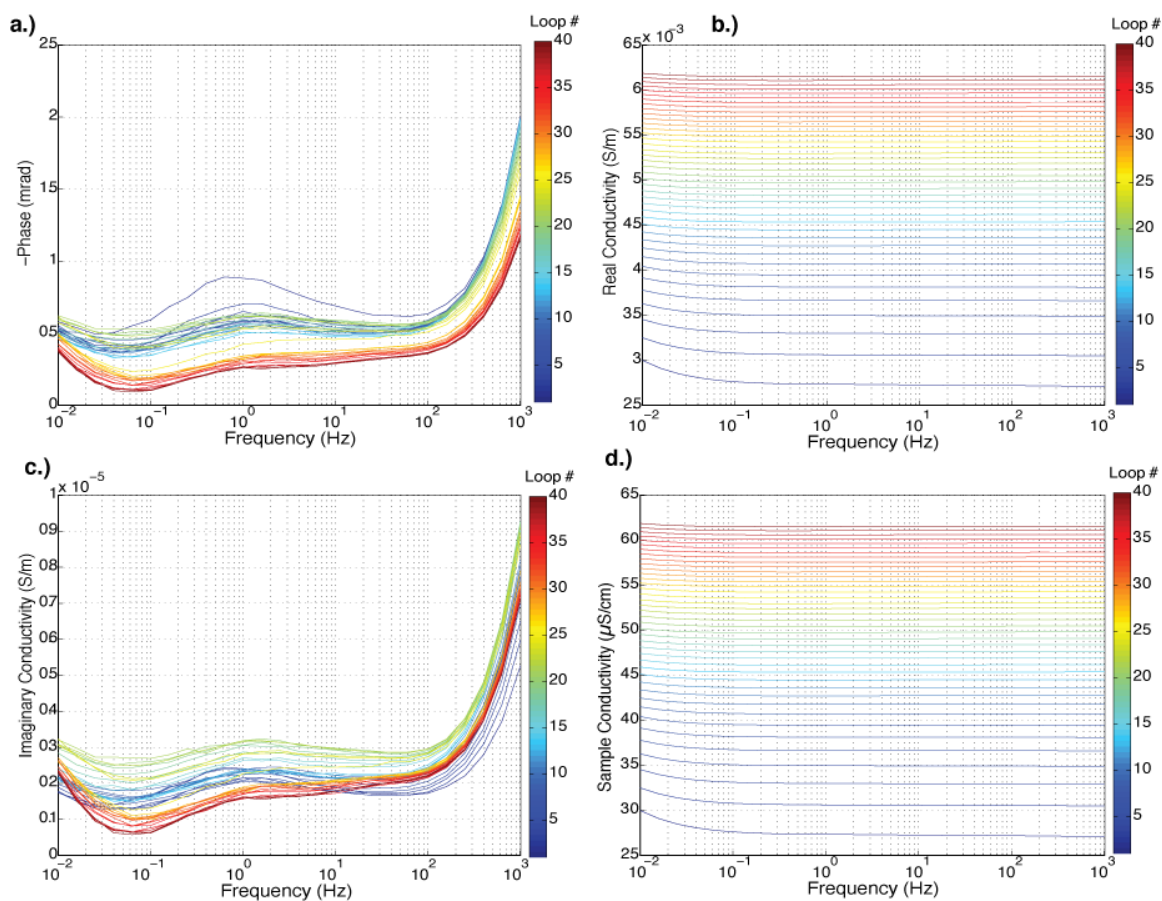


Figure A15: SIP response of 0.07-0.11 mm 0.1 M HCl treated glass beads, sample 3, over 40 frequency sweeps from 1000 to 0.01 Hz with 26 log-spaced steps. a) phase in negative milliradians b) real component of the complex conductivity in S/m c) imaginary component of the complex conductivity in S/m and d) sample conductivity in μ S/cm.

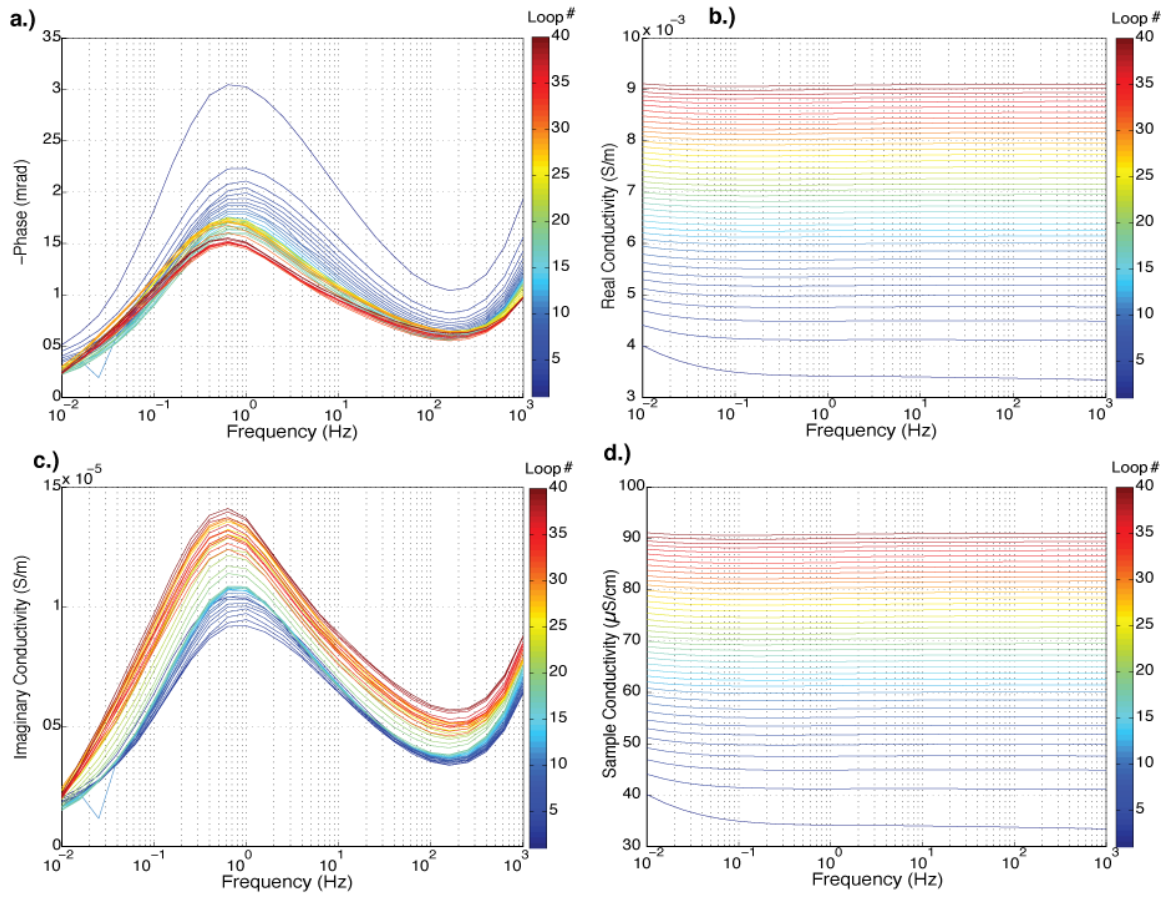


Figure A16: SIP response of 0.07-0.11 mm 1 M NaOH treated glass beads, sample 1, over 40 frequency sweeps from 1000 to 0.01 Hz with 26 log-spaced steps. a) phase in negative milliradians b) real component of the complex conductivity in S/m c) imaginary component of the complex conductivity in S/m and d) sample conductivity in μ S/cm.

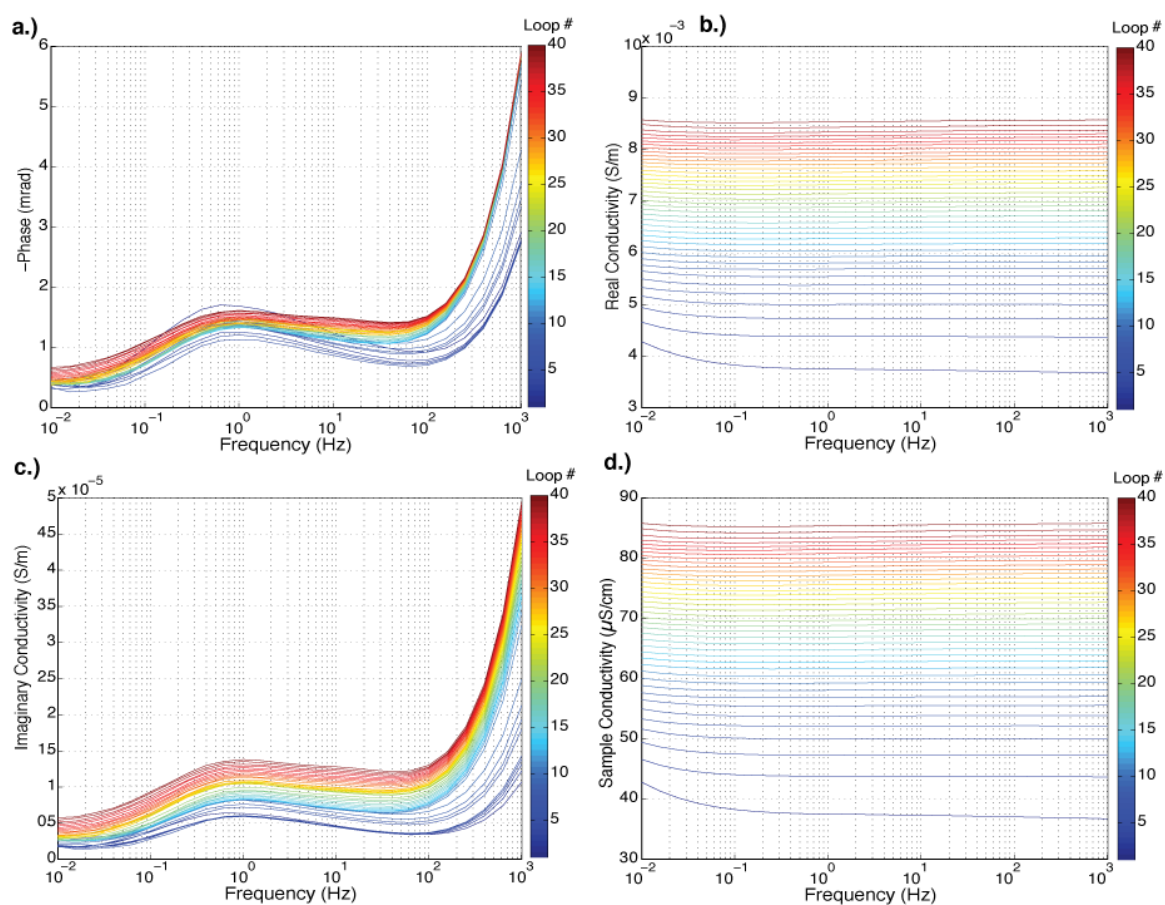


Figure A17: SIP response of 0.07-0.11 mm 1 M NaOH treated glass beads, sample 2, over 40 frequency sweeps from 1000 to 0.01 Hz with 26 log-spaced steps. a) phase in negative milliradians b) real component of the complex conductivity in S/m c) imaginary component of the complex conductivity in S/m and d) sample conductivity in $\mu\text{S/cm}$.

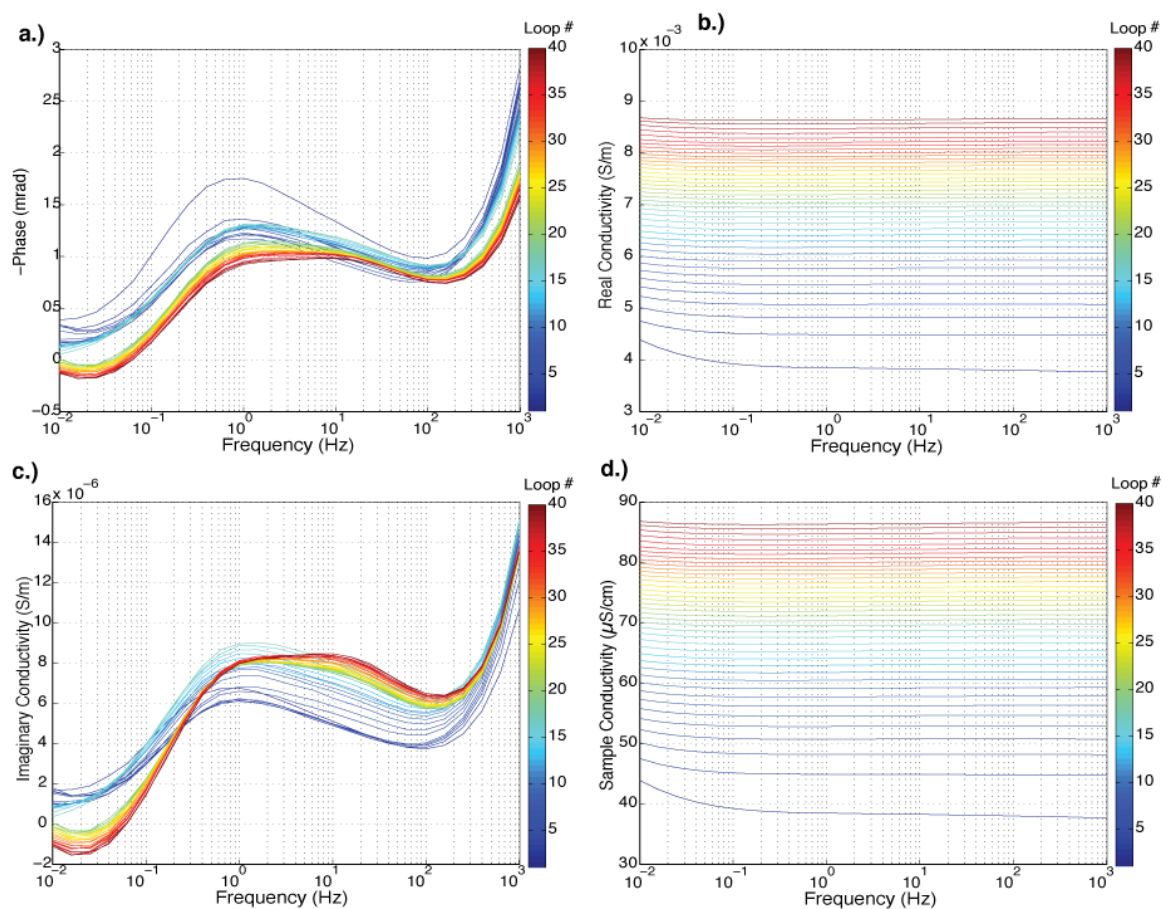


Figure A18: SIP response of 0.07-0.11 mm 1 M NaOH treated glass beads, sample 3, over 40 frequency sweeps from 1000 to 0.01 Hz with 26 log-spaced steps. a) phase in negative milliradians b) real component of the complex conductivity in S/m c) imaginary component of the complex conductivity in S/m and d) sample conductivity in μ S/cm.

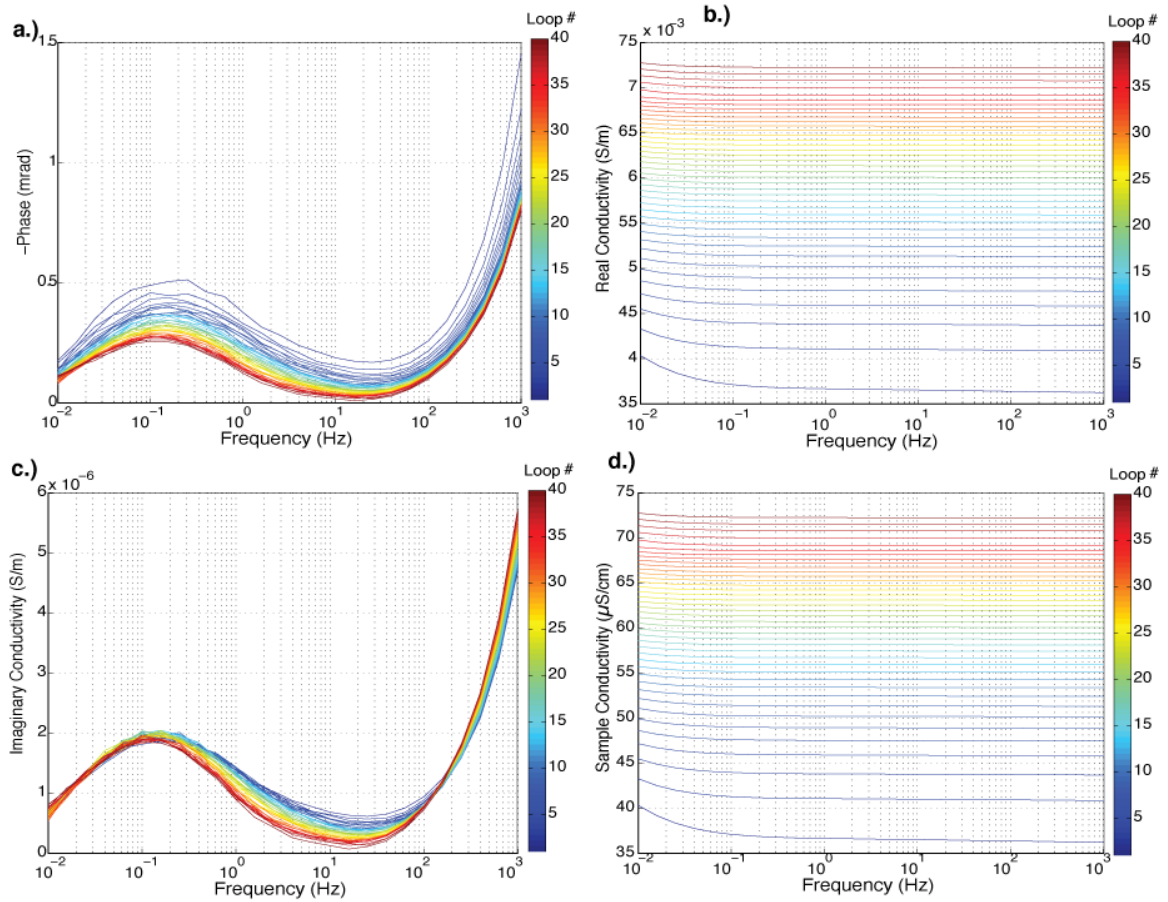


Figure A19: SIP response of 0.2-0.3 mm etching cream treated glass beads, sample 1, over 40 frequency sweeps from 1000 to 0.01 Hz with 26 log-spaced steps. a) phase in negative milliradians b) real component of the complex conductivity in S/m c) imaginary component of the complex conductivity in S/m and d) sample conductivity in μ S/cm.

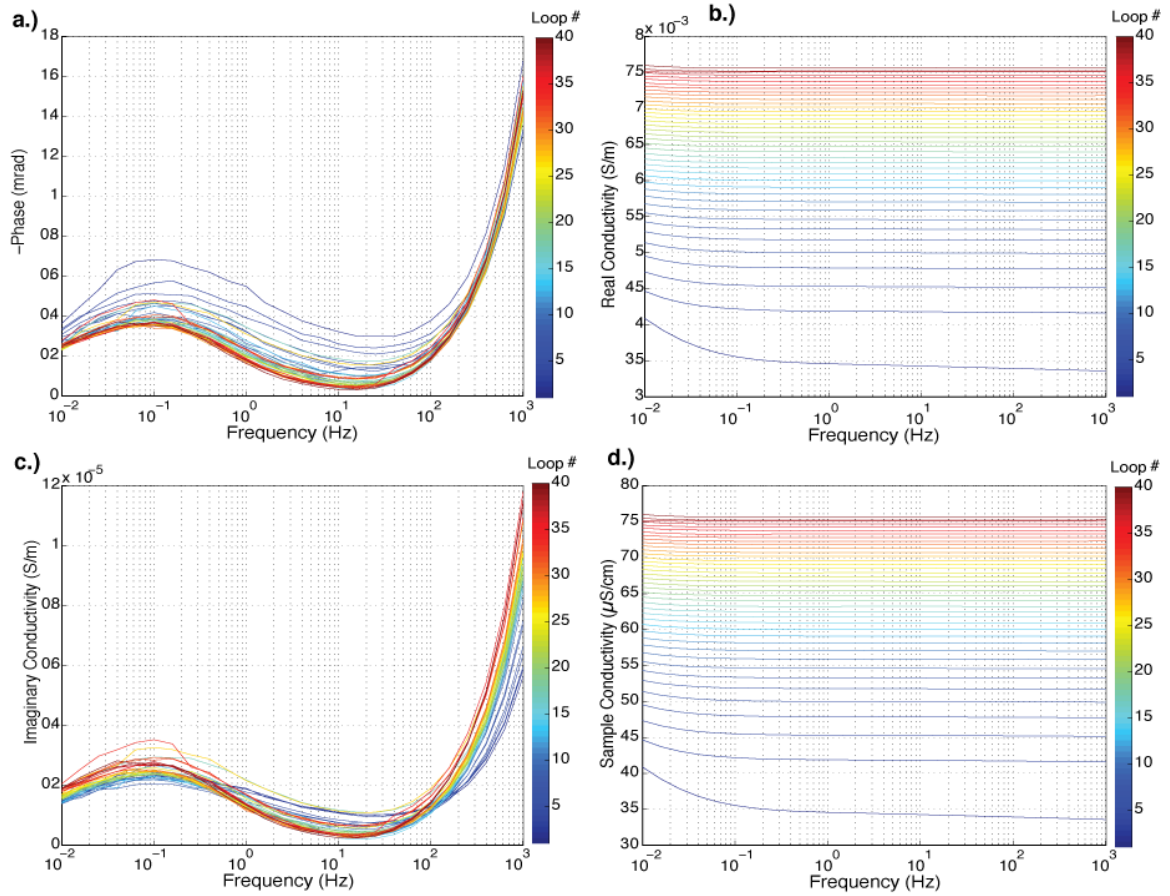


Figure A20: SIP response of 0.2-0.3 mm etching cream treated glass beads, sample 2, over 40 frequency sweeps from 1000 to 0.01 Hz with 26 log-spaced steps. a) phase in negative milliradians b) real component of the complex conductivity in S/m c) imaginary component of the complex conductivity in S/m and d) sample conductivity in μ S/cm.

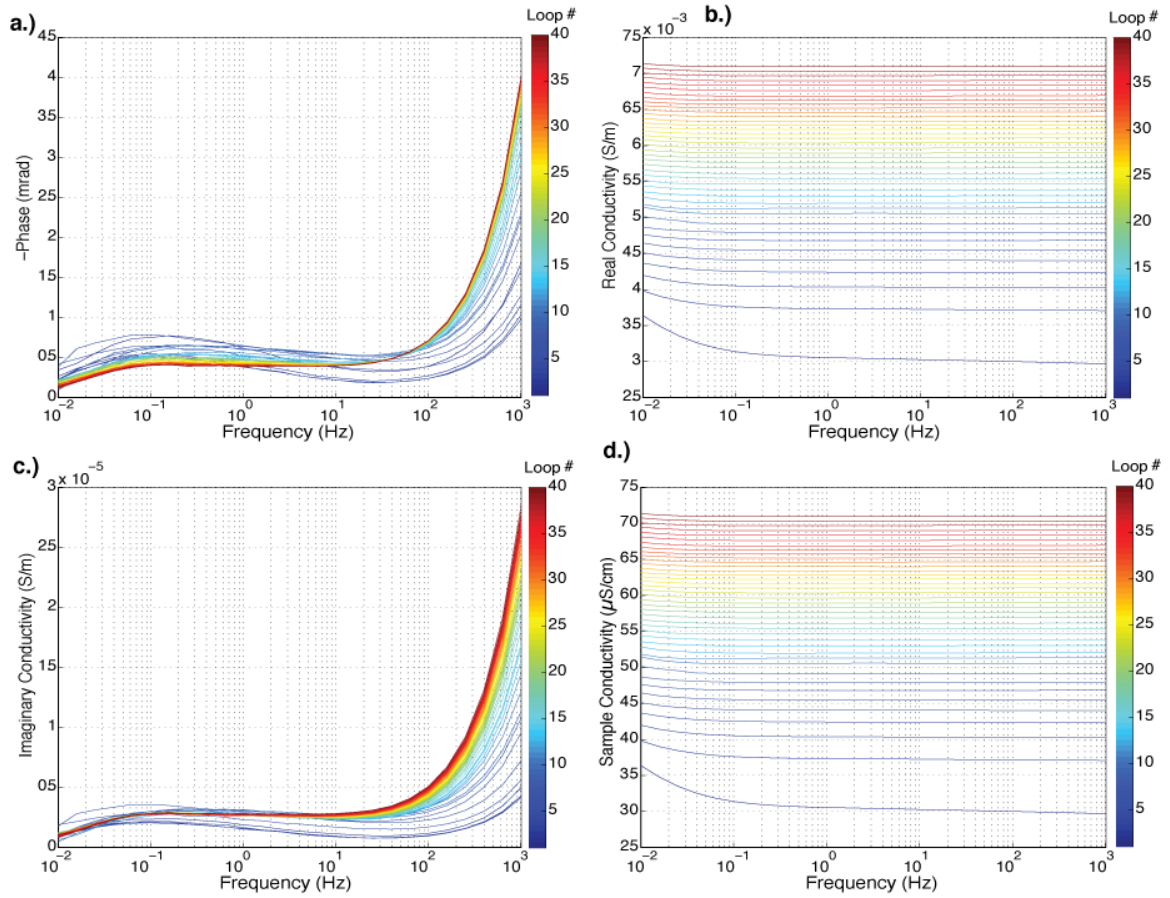


Figure A21: SIP response of 0.2-0.3 mm etching cream treated glass beads, sample 3, over 40 frequency sweeps from 1000 to 0.01 Hz with 26 log-spaced steps. a) phase in negative milliradians b) real component of the complex conductivity in S/m c) imaginary component of the complex conductivity in S/m and d) sample conductivity in μ S/cm.

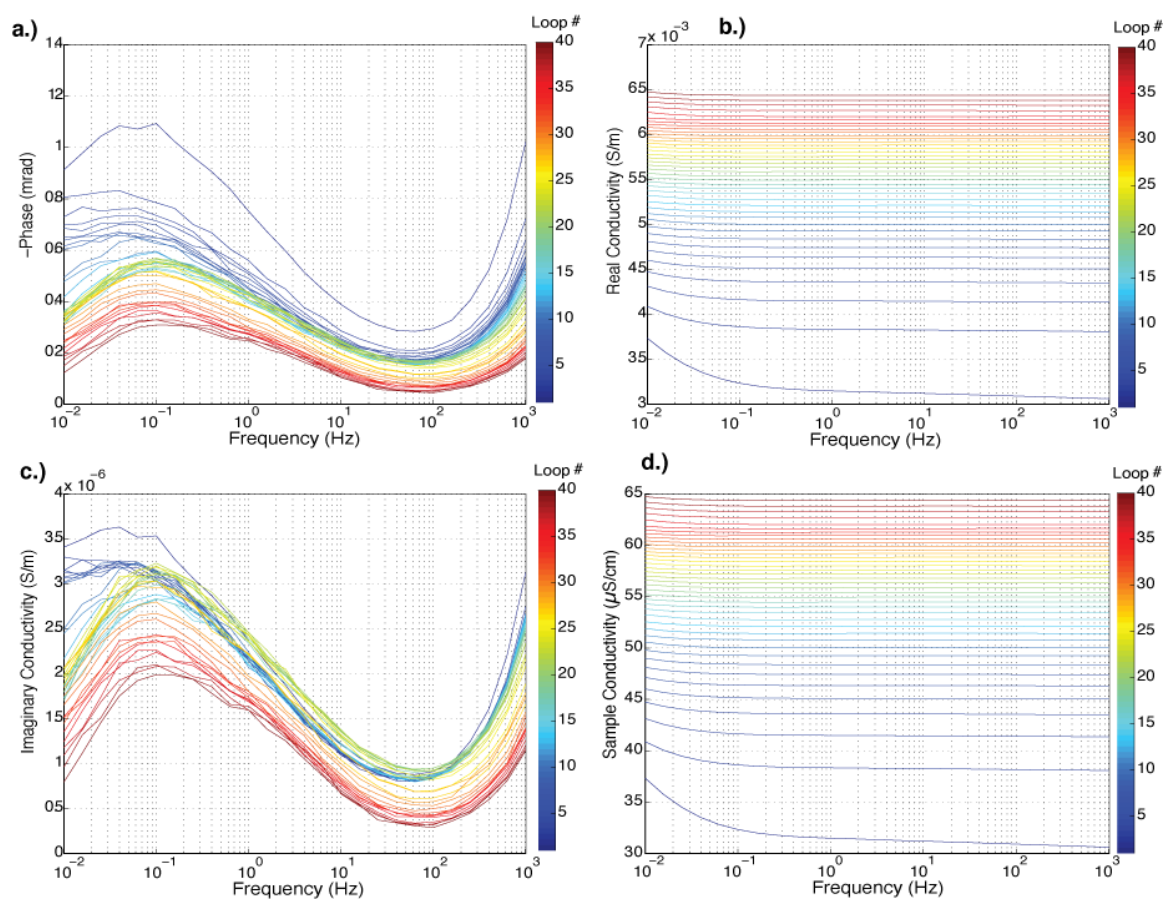


Figure A22: SIP response of 0.2-0.3 mm 0.1 M HCl treated glass beads, sample 1, over 40 frequency sweeps from 1000 to 0.01 Hz with 26 log-spaced steps. a) phase in negative milliradians b) real component of the complex conductivity in S/m c) imaginary component of the complex conductivity in S/m and d) sample conductivity in μ S/cm.

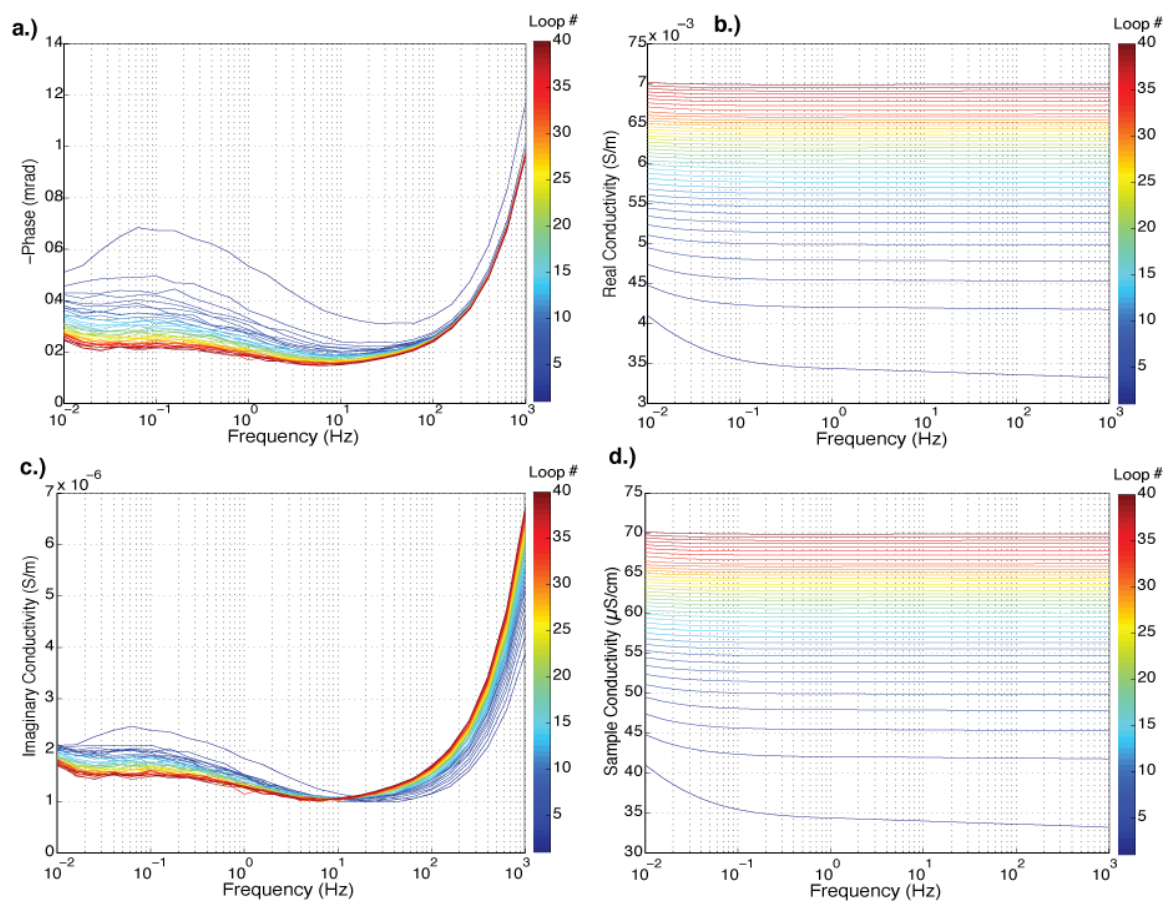


Figure A23: SIP response of 0.2-0.3 mm 0.1 M HCl treated glass beads, sample 2, over 40 frequency sweeps from 1000 to 0.01 Hz with 26 log-spaced steps. a) phase in negative milliradians b) real component of the complex conductivity in S/m c) imaginary component of the complex conductivity in S/m and d) sample conductivity in μ S/cm.

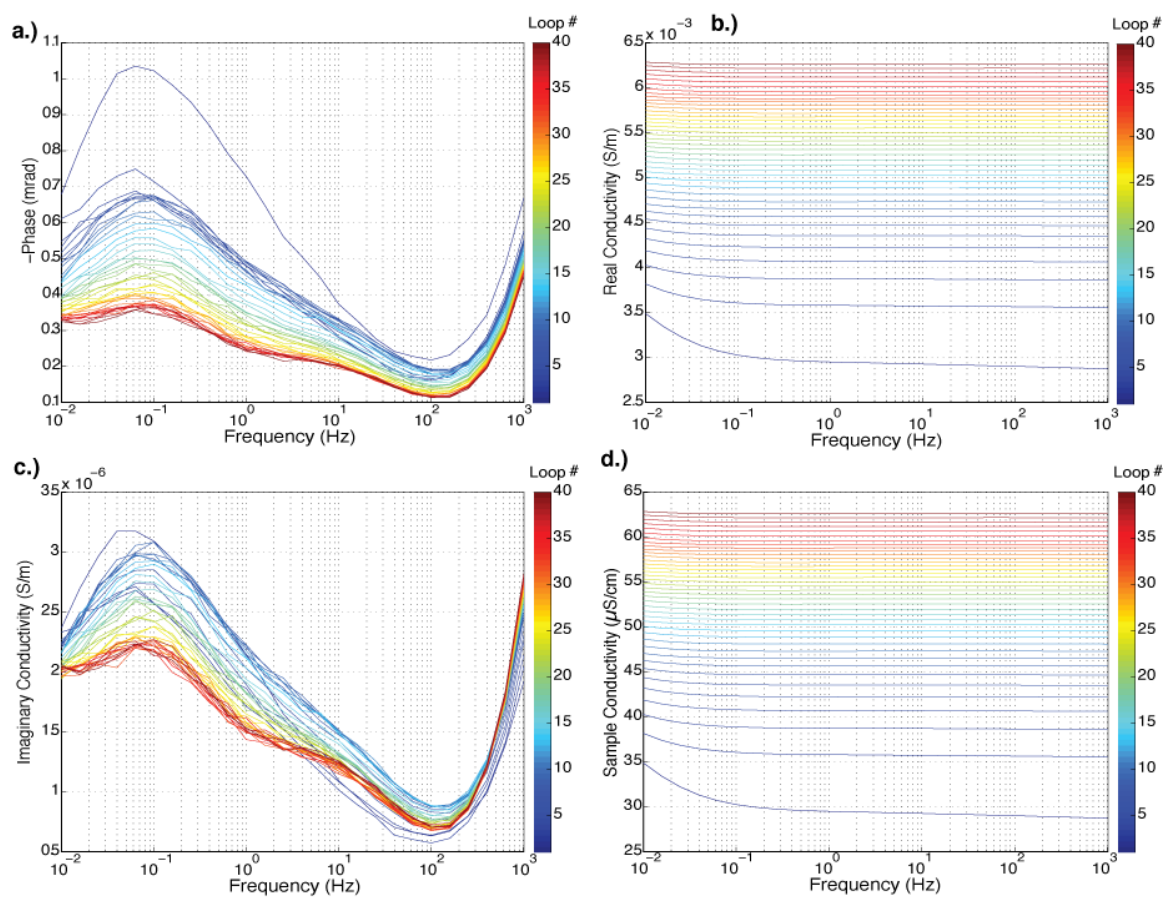


Figure A24: SIP response of 0.2-0.3 mm 0.1 M HCl treated glass beads, sample 3, over 40 frequency sweeps from 1000 to 0.01 Hz with 26 log-spaced steps. a) phase in negative milliradians b) real component of the complex conductivity in S/m c) imaginary component of the complex conductivity in S/m and d) sample conductivity in μ S/cm.

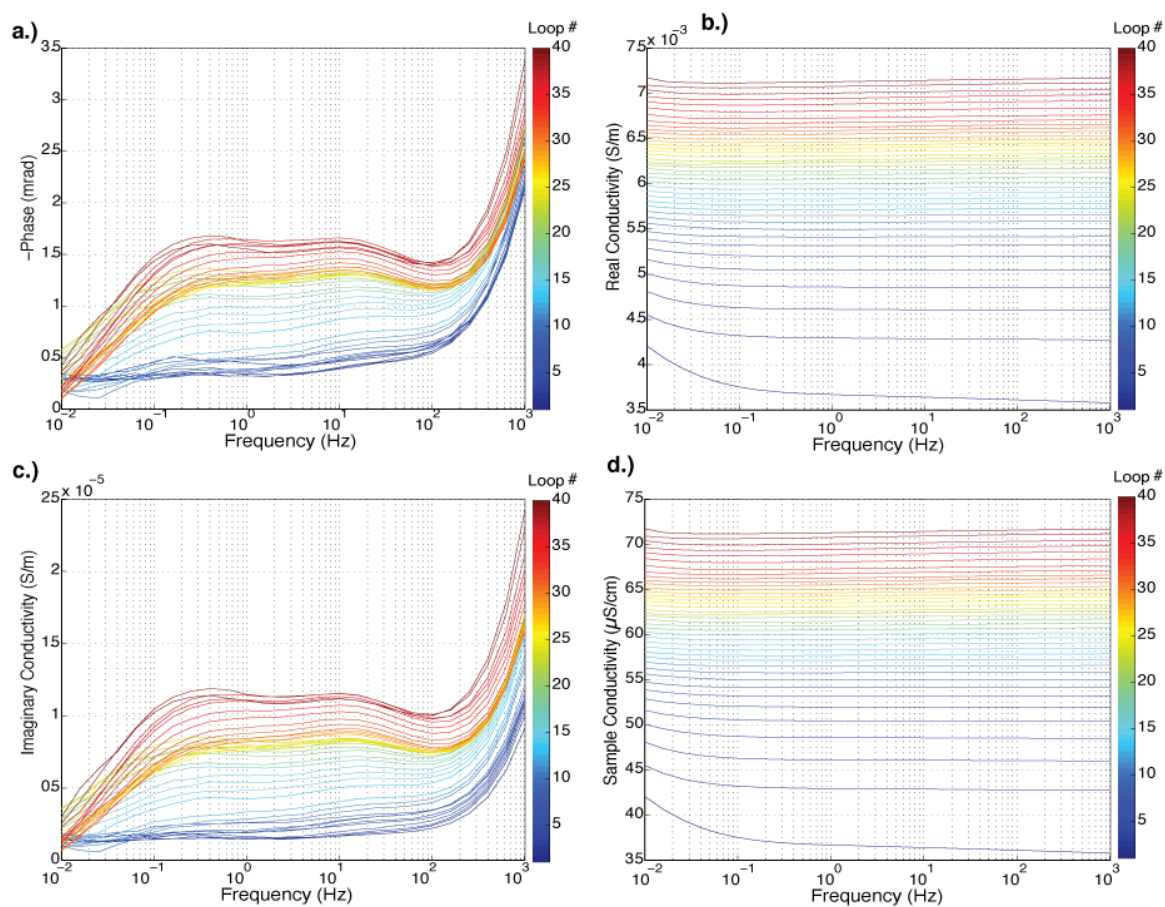


Figure A25: SIP response of 0.2-0.3 mm 1 M NaOH treated glass beads, sample 1, over 40 frequency sweeps from 1000 to 0.01 Hz with 26 log-spaced steps. a) phase in negative milliradians b) real component of the complex conductivity in S/m c) imaginary component of the complex conductivity in S/m and d) sample conductivity in $\mu\text{S/cm}$.

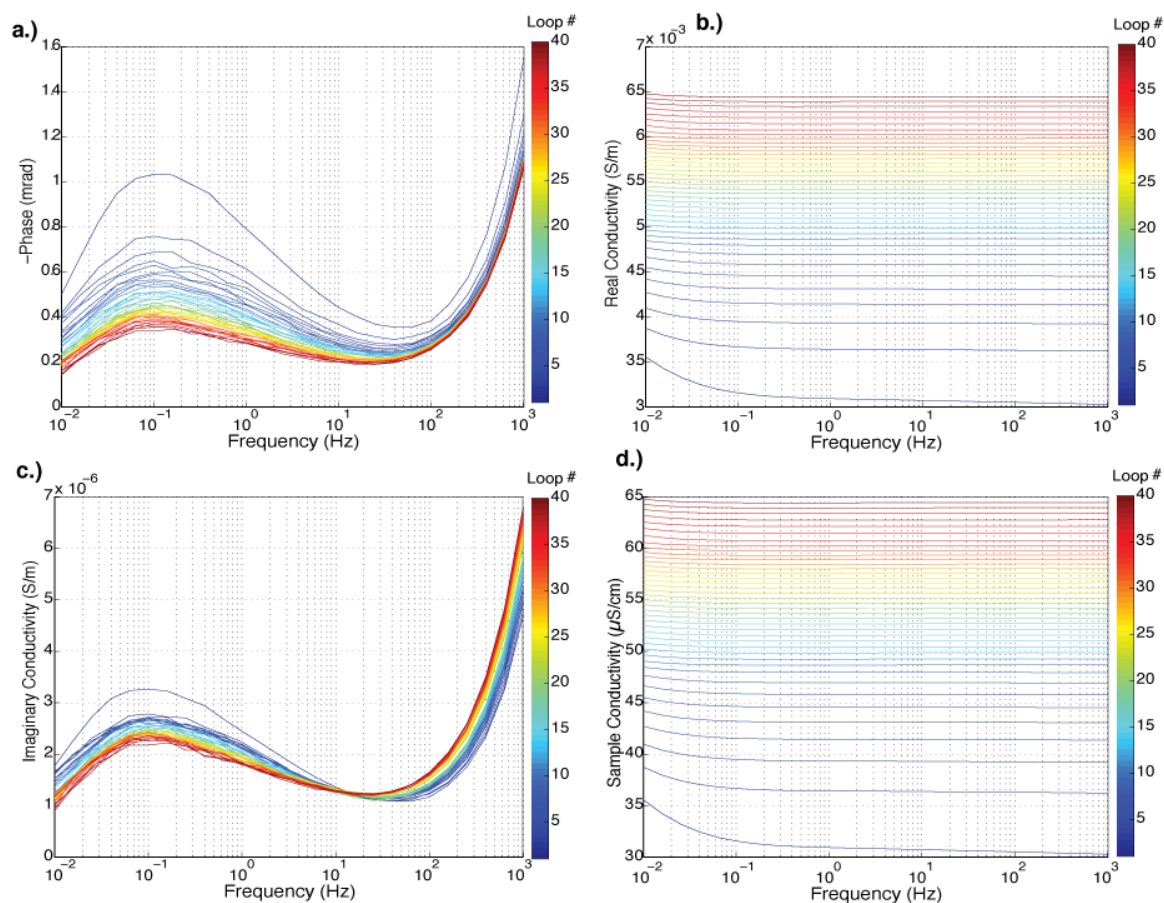


Figure A26: SIP response of 0.2-0.3 mm 1 M NaOH treated glass beads, sample 2, over 40 frequency sweeps from 1000 to 0.01 Hz with 26 log-spaced steps. a) phase in negative milliradians b) real component of the complex conductivity in S/m c) imaginary component of the complex conductivity in S/m and d) sample conductivity in μ S/cm.

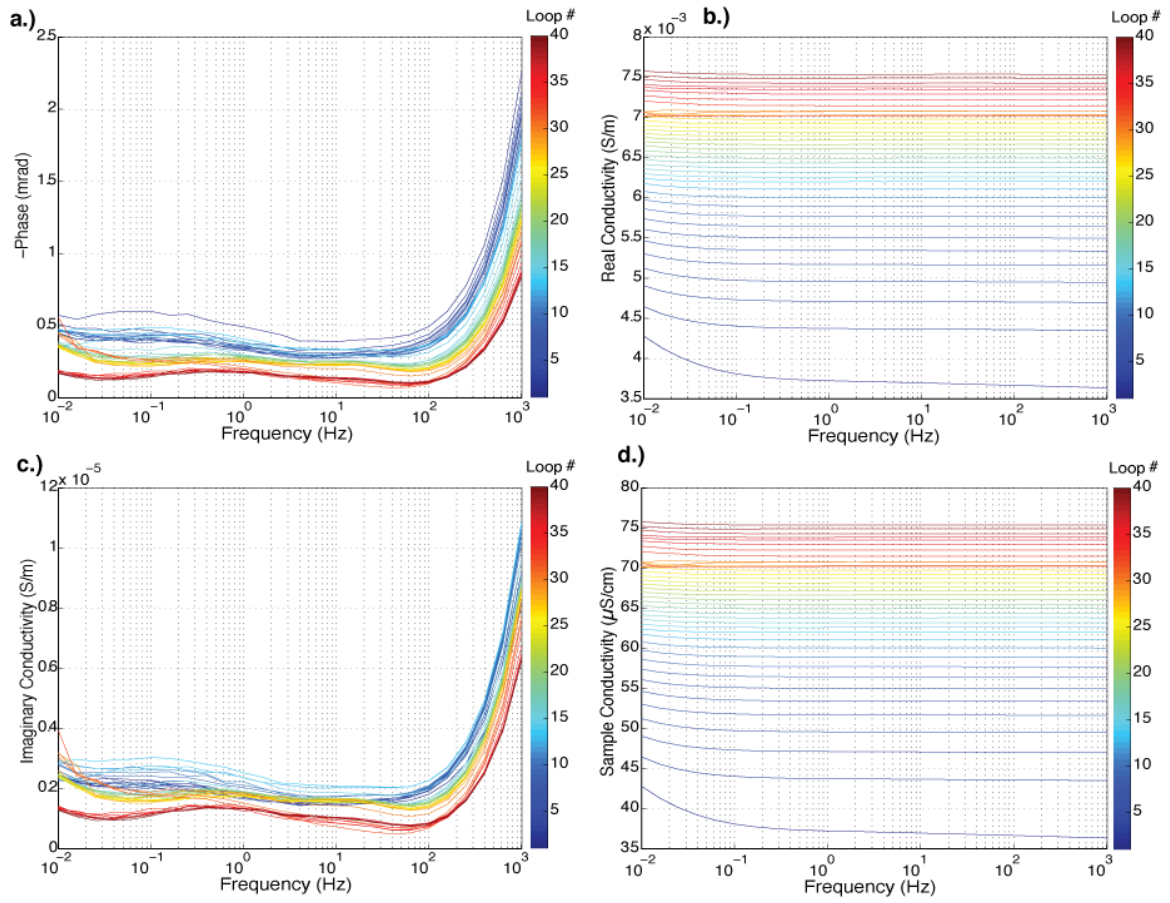


Figure A27: SIP response of 0.2-0.3 mm 1 M NaOH treated glass beads, sample 3, over 40 frequency sweeps from 1000 to 0.01 Hz with 26 log-spaced steps. a) phase in negative milliradians b) real component of the complex conductivity in S/m c) imaginary component of the complex conductivity in S/m and d) sample conductivity in μ S/cm.

CURRICULUM VITAE

David Samuel Wallace

1990	Born October 5 th , McKinney, TX.
2009-2013	Attended Oklahoma State University, Stillwater, OK
2013	B.S. in Environmental Science, Oklahoma State Univ., Stillwater, OK
2013	Staff Scientist Intern, Renova Environmental Services, Ocean Twp., NJ
2013-2015	M.S. Student, Environmental Geology, Rutgers University, Newark, NJ
2014-2015	Student Trainee (Geophysics), US Geological Survey, Fort Worth, TX